POSITRON LIFETIME MEASUREMENTS IN SOME IONIC CRYSTALS AND SOME ALKYLBENZENES

By

CONCEPCION V. SAN JOSE

Bachelor of Science
University of the Philippines
Rizal, Philippines
1959

Master of Science
Purdue University
W. Lafayette, Indiana
1963

Submitted to the faculty of the Graduate College of
the Oklahoma State University
in partial fulfillment of the requirements
for the degree of
DOCTOR OF PHILOSOPHY
July, 1967

POSITRON LIFETIME MEASUREMENTS IN SOME IONIC CRYSTALS AND SOME ALKYLBENZENES

Thesis Approved:

Betty D. Polak
Thesis Adviser

C. Fremont Harris

John B. Wentz

H. Harrington

E. E. Kolumbus

D. D. Dunlap
Dean of the Graduate College

PREFACE

Previous experiments on positron annihilation have demonstrated that the formation and subsequent decay of the electron-positron bound system, the Positronium (Ps) atom, is a property of its immediate surrounding. The investigation of bound-state annihilation may therefore yield information regarding the internal structure of matter. The simplicity of the Ps atom presents the challenge of a new chemical element which may be useful for the understanding of chemical reactions and the nature of chemical bonds.

Due to the discrepancy of existing experimental results, further investigation is required before the usefulness of this approach to solid state problems can be fully assessed. It is the hope of the author that the results obtained herein may be helpful towards the understanding of the electronic structure of matter.

The author wishes to express her sincere gratitude to her major adviser, Dr. Betty L. Pollak, for her invaluable assistance and guidance and to Dr. Rolando Pagilagan and my colleagues, Mr. Ali A. Abdulla, Mr. Raul Nuno and Mr. Alfonso M. Albano for many helpful suggestions and discussions.

Indebtedness is acknowledged to Mr. Wayne M. Adkins of the glass shop and my colleague, Mr. Hsiao-Yuean Li for their help in preparing the de-oxygenated samples. Appreciation is expressed to Miss Amable G. Dorotan and Mr. Henry F. Magalit for their assistance in running the

stepwise linear regression computer program. Recognition is also extended to the University Computing Center for the use of its facilities.

Special appreciation is extended to Miss Salve R. Reusi for proofreading the manuscript and to Miss Carolyn K. Harman for typing this thesis.

TABLE OF CONTENTS

LIST OF TABLES

LIST OF FIGURES

CHAPTER I

INTRODUCTION

Gamma-ray spectroscopy techniques provide methods for the study of the positron annihilation process in several contexts. The first is the investigation of the nature of the positrons and electrons and of their interactions. The discovery of the quasi-stable bound state of an electron-positron pair, Positronium (Ps), confirming earlier theoretical predictions, furnished the physicist with a "chemical" atom in which only electromagnetic forces are present. This atom-like structure served as an ideal system in verifying experimentally the theoretical calculations of quantum electrodynamics.

Positron annihilation in condensed matter has been the subject of a great deal of research. The primary interest lies in investigating the interaction of the positrons with the solid or liquid prior to annihilation, which may yield information regarding the internal structure of matter.

Pair annihilation may also be used in the context in which the decay process serves as an indicator of positron polarization. Whatever information there is available is carried by the annihilation gammas to the observer.

The main disadvantage in these studies lies in the distortion of the electronic configuration by the positron, as is characteristic of most investigation probes in atomic physics. The bound system, Ps, will

not disturb the electron distribution as much, due to its overall electrical neutrality. In this case, the information obtained is limited by the dependence of the annihilation process on the immediate surroundings of this hydrogen-like atom.

Most of the experiments which have been performed fall into three classes (1), which involve measurements of

1) the time distribution of the two-quanta annihilation events

2) two-gamma or three-gamma annihilation rates, the sum of which must be constant from substance to substance

3) the angular correlation between the two photons in 2γ-annihilation.

This work makes use of the first method in determining the positron lifetimes and the relative intensities of the annihilation processes involved.

Several models had been postulated by various researchers to explain theoretically the experimental results so far obtained. No single model, however, is sufficient to explain completely the behavior of positrons in matter.

CHAPTER II

THEORY

Shortly after the development of wave mechanics, Dirac (2) showed that this formalism could be generalized to meet the requirements of Einstein's theory of relativity. Applying his complex equations to the problem of a particle in an electromagnetic field, Dirac was able to give a complete theoretical description of the electron, which was in exact agreement with the negative particle's known properties. The electron's positive energy states were recognized to be the normal states of the electron, while the negative energy states, which stem from the relativistic total energy equation, were attributed to states of the positron, the electron's anti-particle, following its detection in a Wilson Cloud chamber. From this theoretical treatment, the "hole theory" of the positron was formulated.

The Annihilation of Positron-Electron Pairs

Dirac's "hole theory" leads to the simple interpretation: A transition of an electron from a negative energy state to a positive energy state means the creation of an electron-positron pair; the reverse transition means the annihilation of the pair. From energy-mass conservation, the energy given off in pair annihilation is $\geq 2mc^2$. A direct consequence of the interaction of electrons and electromagnetic fields led to the prediction that the rest masses of the pair could be

radiated in the form of electromagnetic energy.

An alternative method which introduces the positron properties from the start is the second quantization of the electron field, in which the wavefunction of the Dirac equation is subjected to a process of quantization similar to the quantization of the radiation field. The quantum conditions must be such that the Pauli principle is fulfilled. This treatment has the advantage that no "infinite sea" of negative energy electrons occurs, and allows for the possibility of creation and annihilation of particles in a natural way (3).

There are essentially three types of pair annihilations whose immediate end products are photons. The first kind is the "annihilation of free electron-positron pairs", which is the annihilation of a free electron and a free positron in relative motion towards one another. The cross-section for this process varies inversely with velocity, so that in the low energy region, it will compete with the second process, the "annihilation from the bound state", which is the annihilation of the pair after formation of the bound system, Positronium. The third type of annihilation takes place in an external field, such as the Coulomb field of a nucleus. This becomes important when positrons annihilate with tightly bound electrons such that the binding to the nucleus cannot be neglected (4). This latter process does not exclude the possibility of one-photon annihilation, since the massive nucleus is present to carry the excess momentum. We may therefore write,

$$e^+ + e^- \longrightarrow n\gamma$$

where n is an integer determined by certain selection rules.

Two-Photon Annihilation Process

In the absence of external fields, simultaneous conservation of energy and momentum requires that the lowest order process yield two photons emitted with equal energy $E = m_o c^2 = 0.51096$ Mev in the center-of-mass system, in opposite directions. Thibaud (5) and Joliot (6) used absorption methods to identify the energy of the annihilation radiation. Using coincidence techniques, these annihilation gammas were shown to be simultaneous and collinear to within 1^o (7,8,9).

High precision spectrometry methods indicated a mean momentum of the center-of-mass of the annihilating pair of about mc/137, indicating that the majority of the positrons reach very low velocity prior to annihilation. At such low velocities, the relative velocities of the two annihilating particles are also very low. In this case, invariance under parity, reflection, and charge conjugation operations allows two-photon decay only from a relative ^1S_o state of the two particles (6,10). An analogous theoretical treatment applied to the three-photon decay shows that the decay is possible only from a relative $^3S_1$ state of the annihilating pair (4).

Annihilation Cross-Sections

The transition probabilities and cross-sections for two-and three-photon annihilation of an electron-positron pair were first calculated by Dirac (2). A simpler method makes use of the famous Feynman diagrams, in which the matrix elements for electromagnetic processes not involving bound states is easily written.

A derivation of the two-photon annihilation cross-section is outlined in the following paragraphs, starting from free annihilation.

The inclusion of the Coulomb wavefunction in the cross-section to be obtained justifies the validity of the application of this calculation for bound state annihilation (4). In calculating for the transition probability, it is necessary to sum over all the final states of polarization of the gamma rays. The Feynman diagrams for the two-photon annihilation process are shown in Figure 1.

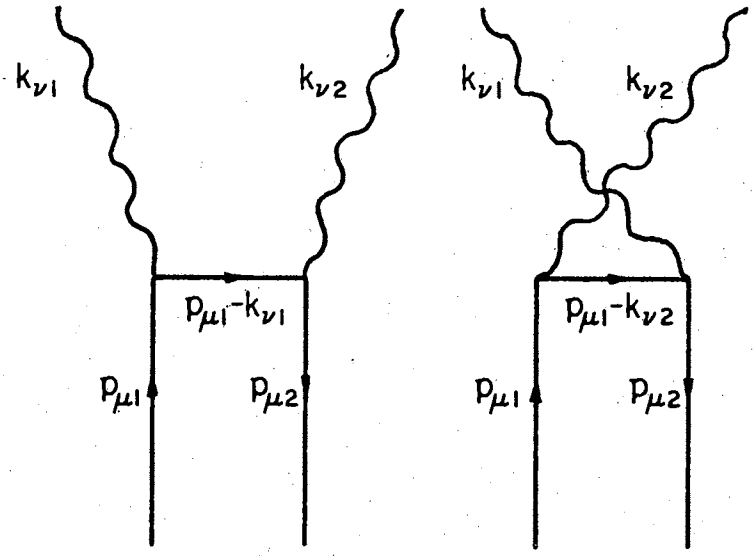

Figure 1. Feynman Diagrams for Two-Photon Annihilation

From the Feynman rules and Figure 1, the amplitude is given by

$$M = -\frac{e^2 2\pi}{\sqrt{\omega_1 \omega_2}} \left[\left(\bar{w}_2 \not{\varepsilon}_2 \frac{1}{\not{p}_1 - \not{k}_1 - m} \not{\varepsilon}_1 w_1 \right) + \left(\bar{w}_2 \not{\varepsilon}_1 \frac{1}{\not{p}_1 - \not{k}_2 - m} \not{\varepsilon}_2 w_1 \right) \right] . \qquad (1)$$

In this notation, w corresponds to the normalized electron spinor wave-

function so that $w^\dagger w = E/m$, the "dagger" notation referring to the hermitian adjoint; $\bar{w} = w^\dagger \gamma_4$, where the γ-matrices satisfy the relation

$$\frac{1}{2}\left(\gamma_\mu \gamma_\nu + \gamma_\nu \gamma_\mu\right) = \delta'_{\mu\nu}$$

where the Greek indices $\mu,\nu = 1, 2, 3, 4$. The delta-metric is given by:

$$\delta'_{\mu\nu} = \begin{vmatrix} -1 & 0 & 0 & 0 \\ 0 & -1 & 0 & 0 \\ 0 & 0 & -1 & 0 \\ 0 & 0 & 0 & 1 \end{vmatrix} .$$

The "slash" notation designates the abbreviation

$$\gamma_\mu A_\mu = \gamma_4 A_4 - \vec{\gamma}\cdot\vec{A} = \not{A}$$

which arises from the definition of the dot product of two four-vectors when the four-dimensional space-time of special relativity is referred to the four real orthogonal axes x, y, z, and t. The four-vectors p_μ and k_ν denote the four-momenta of the electron and photon lines respectively; e refers to the electron charge and m refers to the electron mass; $\hat{\epsilon}$ is the unit vector in the direction of the polarization of the photon. The coefficient of the brackets stems from the normalization factor, $\sqrt{\frac{2\pi}{\omega}}$, of each photon.

Since the positrons are assumed to be thermalized, as will be discussed later, the following approximations are valid: (a) Assume $v \ll 1$ for both positron and electron, and only the fourth components of $p_{\mu 1}$ and $p_{\mu 2}$ are nonvanishing. (b) Assume $v \gg 1/137$ so that the electrostatic attraction may be neglected. The electrostatic effects can be taken into account after the matrix element using plane waves is

obtained.

Applying the laws of conservation of energy and momentum in the approximations stated, the space-time components of the four-momenta of the problem are:

$$
\begin{aligned}
p_{\mu 1} &= 0, \; m \\
p_{\mu 2} &= 0, \; m \\
k_{\nu 1} &= m\hat{k}_1, \; m \\
k_{\nu 2} &= -m\hat{k}_1, \; m
\end{aligned}
$$

where $\hat{k}_1$ is a unit vector in the direction of propagation of the first gamma ray, and where $h/2\pi = c = 1$.

Rationalizing the amplitude,

$$
M = -\frac{2\pi e^2}{\sqrt{\omega_1 \omega_2}} \left[\left(\bar{w}_2 \not{\epsilon}_2 \frac{\not{p}_1 - \not{k}_1 + m}{|p_{\mu 1} - k_{\mu 1}|^2 - m^2} \not{\epsilon}_1 w_1 \right) + \left(\bar{w}_2 \not{\epsilon}_1 \frac{\not{p}_1 - \not{k}_2 + m}{|p_{\mu 1} - k_{\mu 2}|^2 - m^2} \not{\epsilon}_2 w_1 \right) \right] . \qquad (2)
$$

Introducing the approximations into Equation (2), the matrix element becomes

$$
M = -\frac{2\pi e^2}{\sqrt{\omega_1 \omega_2}} \left[\left(\bar{w}_2 \not{\epsilon}_2 \frac{m\gamma \cdot \hat{k}_1 + m}{2m^2} \not{\epsilon}_1 w_1 \right) + \left(\bar{w}_2 \not{\epsilon}_1 \frac{-m\gamma \cdot \hat{k}_1 + m}{2m^2} \not{\epsilon}_2 w_1 \right) \right] .
$$

The terms

$$
\not{\epsilon}_2 m \not{\epsilon}_1 + \not{\epsilon}_1 m \not{\epsilon}_2 = 2m \hat{\epsilon}_1 \cdot \hat{\epsilon}_2
$$

do not induce transitions between electron and positron states since they do not contain γ-matrices; consequently they can be omitted. Therefore,

$$M = -\frac{\pi e^2}{m^2} \left[\bar{w}_2 \left(\not{\epsilon}_2 \gamma \cdot \hat{k}_1 \not{\epsilon}_1 - \not{\epsilon}_1 \gamma \cdot \hat{k}_1 \not{\epsilon}_2 \right) w_1 \right] .$$

Choosing conveniently the positive directions of $\hat{\epsilon}_1$, $\hat{\epsilon}_2$ and $\hat{k}_1$, the matrix element can be written in terms of the spinors as:

$$w^{\dagger}_{(4)} \gamma_5 w_{(1)} = +1$$
$$w^{\dagger}_{(3)} \gamma_5 w_{(2)} = -1 ,$$

the first of which corresponds to the nonrelativistic annihilation of a pair $\alpha_- \beta_+$, electron with spin up, positron with spin down; the second applies to the pair annihilation $\alpha_+ \beta_-$, electron with spin down, positron with spin up. Only singlet pairs annihilate due to the opposite signs of the matrix elements. With the unit vectors in the directions chosen and applying anticommutation relations,

$$M = \frac{2\sqrt{2}\,\pi e^2}{m^2} .$$

The density of final states in this calculation is

$$\frac{2k_1^2\, dk_1}{8\pi^3} \frac{d\Omega_1}{2dk_1} = \frac{d\Omega_1}{8\pi^3} k_1^2 = \frac{d\Omega_1}{8\pi^3} m^2$$

where a factor of 2 in the numerator takes into account the two polarizations, and $dE_o = 2dk_1$. The gamma rays are indistinguishable and summing both diagrams, the integration over $d\Omega_1$ is equal to 2π.

The transition probability for unit-density singlet electron-positron plane waves is

$$\lambda_s = 2\pi \frac{2\pi}{8\pi^3} m^2 \left(\frac{2\sqrt{2}\ \pi e^2}{m^2} \right)^2 = \frac{4\pi e^4}{m^2} \quad . \tag{3}$$

Averaging over the four spin orientations, the singlet annihilation cross-section for free collision reduces to

$$\sigma_s = \frac{\pi}{v} \frac{e^4}{m^2} \left| \Psi(0) \right|^2 .$$

Including all constants, one obtains

$$\sigma_s = \pi \frac{c}{v} \left(\frac{e^2}{mc^2} \right)^2 \left| \Psi(0) \right|^2 = \pi r_o^2 \frac{c}{v} \left| \Psi(0) \right|^2 , \tag{4}$$

where r_o is the classical electron radius. The probability density $\left| \Psi(0) \right|^2$ is unity if Coulomb attraction is neglected. Otherwise, it can be computed from Coulomb wavefunctions.

For the S state of Ps, of total quantum number n,

$$\left| \Psi(0) \right|^2 = \frac{1}{\pi} (2na_o)^{-3} , \tag{5}$$

where $a_o = r_o/\alpha^2$, α being the fine structure constant. The factor of 2 arises from the correction for the reduced mass (11). The mean-life of the singlet ground state of Ps states, in the limit of small velocities is

$$^1\tau_{para} = 1.25 \times 10^{-10}\ n^3 \text{ sec.} \tag{6}$$

where n = 1.

A similar approach to the annihilation through three-photon

emission yields a cross-section

$$\sigma_t = \frac{4}{3}(\pi^2 - 9)\,\alpha\, r_o^2 \frac{c}{v} \tag{7}$$

and

$$^3\tau_{ortho} = 1.4 \times 10^{-7}\, n^3 \text{ sec.} \tag{8}$$

where n = 1 for ground state Ps. Due to the multiple character of three photon annihilation, the triplet state will have a longer lifetime than the singlet.

For states of non-zero angular momenta, the annihilation probability is negligible compared to the probability of optical transition, whereas annihilation predominates for zero angular momentum. The spin-averaged cross-section ratio is

$$\frac{\sigma_{ortho}}{\sigma_{para}} = \frac{\frac{3}{4}\sigma_t}{\frac{1}{4}\sigma_s} = 3\left(\frac{^1\tau_{para}}{^3\tau_{ortho}}\right) = \frac{1}{372} \,. \tag{9}$$

Positron Lifetime in Matter

In general, the annihilation rate of slow positrons in matter is given by the equation

$$\tau^{-1} = \lambda = C_s\Psi_s^2 + C_t\Psi_t^2 \,, \tag{10}$$

where Ψ_s^2 is the density of electrons with "antiparallel" spin at the average position of the positron; i.e., annihilation from the singlet spin state. Ψ_t^2 is the same quantity for triplet spin orientation. C_s and C_t are fundamental interaction rates in the singlet and triplet

states. In the plane wave approximation (12,13),

$$C_s = 4\pi c\left(\frac{e^2}{mc^2}\right)^2 = 3 \times 10^{-14} \text{ cm}^3/\text{sec.} \quad (11)$$

and

$$C_t = 4\pi c\left(\frac{e^2}{mc^2}\right)^2 \frac{4\alpha}{9\pi}(\pi^2 - 9)$$

$$= \frac{1}{1115} C_s = 2.7 \times 10^{-17} \text{ cm}^3/\text{sec.} \quad (12)$$

Neglecting the effects of Coulomb forces, $\Psi_s^2 = (1/4)n_e$ and $\Psi_t^2 = (3/4)\ n_e$, where n_e is the number of electrons per cubic centimeter of matter. If Coulomb interaction is considered, but one still assumes that the positrons move freely through the medium, the above equations are still valid where n_e now stands for an "effective" number of electrons.

Generalizing, the annihilation rate in collisions should be proportional to the density of available electrons, and therefore for a particular substance, to the density. Deutsch (14) demonstrated the fact that the proportionality of annihilation rate and density was not satisfied, and established the fact that annihilation of slow positrons sometimes involves positronium formation.

CHAPTER III

REVIEW OF THE LITERATURE

Positron Lifetimes

Some general features have been demonstrated in the study of positron annihilation in matter. Analyses of time distribution spectra show that most metals exhibit only a short lifetime ($\tau_1 \sim 10^{-10}$ sec.), whereas molecular compounds are characterized by the presence of τ_1 as well as a well-defined linear "tail" on the curve corresponding to an exponential decay of markedly longer lifetime ($\tau_2 \sim 10^{-9}$ sec.). The appearance of two distinct meanlives implies that two annihilation processes are present, and that they are mutually exclusive (15).

Many properties of pair annihilation are understood on the assumption that positrons in the sample under study are thermalized before they interact with the electrons of the substance. The validity of the assumption made in the derivation of the annihilation cross-section in Chapter II may be seen from the following paragraphs.

Calculations on positron thermalization time (16,17,18) in metals have been carried out. The generally accepted value is that of Lee-Whiting (18), who reported a thermalization time of $\sim 3 \times 10^{-12}$ second. Since the experimental positron lifetimes in metals are all of the order of 10^{-10} second, it is safe to assume that positrons are thermalized prior to annihilation.

Angular correlation experiments on the 2γ-annihilation process in metals can be explained only if one assumes that most of the positrons are thermalized and diffuse freely in the conductor. Due to the similarity of experimental results in metals and nonconductors, the assumption of thermalized positrons is reasonable.

The Short Lifetime and Its Interpretations. Positrons entering a condensed medium lose energy mainly by inelastic collisions, and at low energies, direct annihilation and Ps formation become competing processes. This gives rise to the short lifetime component, τ_1, which appears to be insensitive to lattice characteristics. Mostly metals comprise the class of compounds which exhibit only the prompt decay mode.

A cross-section for the annihilation of a slow positron by a free electron is given by Equation (4), in which the probability density $|\Psi(0)|^2$ is unity. In the free electron theory approximation the predicted decay rate of positrons annihilating in a material of density, D, and atomic mass, A, is

$$\lambda = \frac{1}{\tau} = \sigma v N_e \qquad (13)$$

where N_e is the density of outer shell electrons. This leads to

$$\tau = 2.2 \times 10^{-10} \frac{A}{DZ_{eff}} \text{ sec.}, \qquad (14)$$

where Z_{eff} is the number of outer electrons per atom, since presumably only the valence electrons are effective in the annihilation process. This assumption, however, is unable to account for the constancy of τ_1 in most metals. Interpreting the lifetimes in terms of Ps formation is

ruled out, since annihilation from bound states leads to an unobserved long lifetime.

The discrepancy between the experimental results and the theoretical predictions may be interpreted by assuming that electrons "swarm" around the positron when it reaches low energies. If this were true, then Coulomb attraction between members of the pair becomes important in the computation of σ and nuclear repulsion confines the positron to a region where the electron density is not simply equal to its average value.

In explaining the negative results of the experiment carried out by Mandansky and Rasetti (19), which dealt with the detection of thermal positrons diffusing through thin metal foils, Ferrell (20) pointed out that there is a lowering of positron energy as a result of electron-positron correlation. The electrons are free to interfere with any Ps atom which might be formed and can either strongly modify the Ps or prevent its independent existence.

The Anomalous Lifetime. In most molecular substances, a complex decay is observed, where the short-lived component is due to para-Ps decay and free annihilation. The anomalously slow component is attributed to collision-induced two-photon annihilations of triplet Ps. Positrons slowing down in the sample may form triplet Ps atoms which are destroyed mainly by conversion to the singlet state through collisions with the atoms of the sample material (15). Assuming that exchange collisions are responsible for triplet-to-singlet conversion, three-photon annihilation will occur in a fraction of the long lifetime given by the ratio of its observed lifetime to the lifetime of triplet Ps in the sample. The experimental results of Pond (21) are consistent with this

hypothesis. This mechanism appears to be ruled out in insulators since the electrons occupy closed shell configurations, in contrast to their free states in metals.

On the other hand, Garwin (17) explained the slow mode of decay by postulating the formation of ortho-Ps and its subsequent annihilation by the "pickoff" mechanism, whereby the positron in triplet Ps annihilates with an electron of opposite spin from a neighboring molecule. This annihilation process is described in a later paragraph.

There are experimental evidences (22,23,24) that the formation of positronium compounds such as e^+Cl^- or $(e^+e^-)Cl$ is another process which competes with the "pickoff" mechanism. These compounds may not necessarily be thermodynamically stable so long as they survive long enough to permit annihilation of the positron with an atomic electron. In the case of the halogens Cl_2 and Br_2, the compound state dissociates by collisions in a time comparable with the annihilation time (22).

The long meanlife, τ_2, is dependent on temperature, molecular composition, physical state and other properties of the material, in which positrons annihilate. A valid generalization for the class of compounds exhibiting τ_2 is that if electron exchange takes place, it would occur only within individual molecules and that any covalent forces which may be present between molecules are repulsive.

The intensity of the slow mode of decay, I_2, is associated with the amount of positrons forming positronium. Due to the multiplicity of the triplet state, 3/4 of all positrons forming a bound state will be in the ortho-state, decaying with a lifetime $\sim 10^{-9}$ second. It has been observed (25) that I_2 is subject to considerable variation and is affected by a number of external factors such as temperature and pressure.

Experiments on water and ice confirm the hypothesis that the temperature effect on I_2 is due to variation of density with temperature. The decrease of positronium formation at low temperatures may be explained on the basis of the fact that lowering the temperature increases the density, so that less space is available to the Ps atom effecting a weaker binding. This would result in raising the lower end of the "Ore-gap".

a. The "Ore-Gap" Model

The formation of Ps atoms is easily understood by means of the "Ore-gap" which was first applied to gases (26) to explain the existence of Ps atoms. With certain modifications, this model has been applied to liquids and solids. The binding energy of the Ps atom is 6.8 ev., which is half the ionization potential of the hydrogen atom, resulting from the reduced mass effect. Calling V_1 the ionization energy of the gas molecules and V_e the minimum positron kinetic energy, there exists an energy range in which Ps formation is most likely if $V_e > V_i - 6.8$ ev. This range of positron kinetic energy is called the "Ore-gap", and is determined by

$$V_i - 6.8 < E < V_e \quad . \tag{15}$$

For energies below the "Ore-gap", the positron has insufficient energy to capture an electron. Above the "Ore-gap", energy loss by inelastic collisions is predominant.

b. Pickoff Mechanism

In interpreting the anomalous lifetime in nonmetals, Garwin (17) suggested that the decay is not due to triplet-to-singlet conversion, but by annihilation of the positron, after formation of triplet Ps, with an electron from a neighboring molecule with a relative singlet

spin orientation. This mechanism has come to be known as the "pickoff" annihilation process, and is the generally accepted explanation for the existence of the τ_2-component in nonconductors and insulators.

This electron pickoff process depends on the overlap of the positron component of the Ps wavefunction with the lattice wavefunction. It is assumed that the Ps wavefunction in a lattice is not deformed to an extent that Ps becomes pressure self-quenched or unstable, so that τ_2 is a measure of the lattice-Ps interaction and its dependence on lattice properties (27).

The decrease in the pickoff annihilation rate with increasing temperature has been shown to be a quantum mechanical effect. A thermalized Ps atom has a de Broglie wavelength 2-3 orders of magnitude larger than the dimensions of the "free volume" per molecule accessible to Ps in a typical molecular lattice. Therefore, one can think of the Ps as an "injected" exciton of high mobility, with a radius comparable to intermolecular spacings (20).

Assuming that Equation (10) describes the decay rate for the pickoff process, Gerholm (28) gives a rough estimate of the electronic quenching cross-section, σ_e, by this mechanism. He obtains

$$\sigma_e \sim \pi r_o^2 \; \frac{1}{2} C_s \frac{1}{\pi r_o^3} \cdot \frac{2r_o}{v'} = \frac{C_s}{v'} \tag{16}$$

where r_o is the classical electron radius, v' the velocity of the external electron and C_s given by Equation (11). The velocity v' is approximated by

$$v' \sim \frac{1}{137} \cdot \frac{Z}{n_{eff}} \cdot c \tag{17}$$

where Z is the atomic number and n_{eff} the effective number of electrons.

The molecular quenching cross-section σ_m corresponding to σ_e and μ valence electrons is given by

$$\sigma_m = \mu \sigma_e \quad . \tag{18}$$

The annihilation rate then becomes

$$\lambda_2 \sim n_{eff} v \sigma_e \quad , \tag{19}$$

where v is the velocity of the Ps atom, presumably thermal at room temperature.

Assuming λ_1 is given by

$$\lambda_1 = \frac{1}{4} \cdot \frac{C_s N_o \mu \Delta}{A} \quad , \tag{20}$$

where Δ is the density of the material, the τ_2/τ_1 ratios obtained were larger than experimental values by almost a factor of 2. Gerholm concludes that the inner shell electrons make a relatively more appreciable contribution to the pickoff decay rate than to direct annihilation.

c. Free Volume Model

Some features of pickoff quenching seem to be explained by the "free volume" model (27) which correctly predicts the dependence of τ_2 on pressure, temperature and phase change. This model fails, however, to explain the increase of τ_2 in ice upon melting.

Neglecting Ps and lattice mutual polarization and assuming that the Ps atom moves in a field described by square potentials U_o, the electron pickoff rate in the Wigner-Seitz approximation is given by

$$\gamma_p = \frac{\pi r_{ex}^2 \; c \; \rho_o}{1 + F\,(U_o,\, r_{ex},\, r_1)} \quad . \tag{21}$$

In this equation, ρ_o is the electron density, r_{ex} the radius corresponding to the "excluded" volume (V_{ex}) centered in a cell volume V_1 described by the radius r_1. The "free volume" available to the Ps atoms is $V_1 - V_{ex}$, which is temperature dependent.

The function $F\,(U_o, r_{ex}, r_1)$ depends upon the geometry of the lattice and is a function of the scattering parameter

$$P_o r_{ex}^2 = \left(\frac{4m}{\hbar^2}\right) \; U_o r_{ex}^2 \quad . \tag{22}$$

The theoretical expression for τ_2 is given by

$$\tau_2 = \frac{1}{(\pi r_{ex}^2 \; c \; \rho_o)} \left[1 + F\,(U_o, r_{ex}, r_1)\right] . \tag{23}$$

Brandt et al.(27) conclude that intermolecular distances set an upper limit to the lifetimes of ortho-and para-Ps, since in small confinements the internal lattice pressure is exceeded by the Ps pressure against the lattice. The molecules would yield before they can accomodate Ps in such small volumes.

d. Quenching Effects

The term "quenching" refers to processes which cause Ps atoms in the triplet state to decay at a rate faster than their natural decay rate of 0.7×10^7/second. The quenching effects of impurities, external magnetic field and external electric field on Ps atoms demonstrate that ortho- to para-Ps conversion may be accomplished by several mechanisms.

The quenching process due to the presence of an applied magnetic

field may be understood on the basis of the second order Zeeman effect, due to the mixing of singlet and triplet components. A field, B, displaces the two sub-states with m = 0 with respect to the unperturbed state by an amount

$$hf = \pm \frac{1}{2} \Delta W \left[(1 + y^2)^{\frac{1}{2}} - 1 \right] \tag{24}$$

where $y = 4\mu_e B/W$ and μ_e is the electron magnetic moment and ΔW is the splitting. The m = 0 triplet state contains an admixture of the singlet by the amount $\frac{a^2}{(1 + a^2)}$,

where

$$a = y^{-1} \left[(1 + y^2)^{\frac{1}{2}} - 1 \right] \approx \frac{2\mu_e B}{\Delta W} \quad . \tag{25}$$

This admixture allows two-photon decay, in which the external magnetic field absorbs the unbalanced angular momentum. The relative probability of this two-photon annihilation is $a^2/(\lambda_t/\lambda_s + a^2)$ where λ_t and λ_s are the unperturbed annihilation rates of the triplet and singlet states, respectively (29).

The application of an external electric field increases the amount of Ps formed, because of the acceleration of any free positrons present back into the "Ore-gap", resulting in a decrease in the two-photon yield. This process has provided a method for estimating the cross-sections of positrons in inert gases, since the number of positrons accelerated back into the "Ore-gap" is a function of the scattering mean free path (12).

The addition of impurities such as NO and NO_2 which contain

unpaired electrons show that the conversion may be explained by exchange of electrons of opposite spins. In collisions between a paramagnetic molecule and a Ps atom, aside from compound formation or "pickoff" quenching, spin change is induced in the Ps atom by either the "spin-flip" process or change in Ps spin without energy exchange (30). The "spin-flip" mechanism results from the direct exchange of the unpaired electron of the paramagnetic molecule with the electron of the Ps atom. The equation which shows total spin momentum conservation, may be written as

$$M(\uparrow) + o\text{-}Ps(\downarrow\overset{+}{\uparrow}) \longrightarrow M(\downarrow) + p\text{-}Ps(\uparrow\overset{+}{\downarrow}), \quad (26)$$

where M stands for the molecule, the arrow indicates electron spin orientation, and the crossed-arrow, that of the positron.

If no energy exchange takes place during the collision, a molecule of spin **S** may change the Ps spin so that

$$M(S) + o\text{-}Ps \longrightarrow M(S) + p\text{-}Ps \cdot \quad (27)$$

From angular momentum conservation this process is not allowed for **S** = 0.

Magnetic interaction between the Ps atom and the field of the paramagnetic molecule causes transitions with a conversion rate not much greater than 10^5 sec.$^{-1}$. The ortho-Ps self-annihilation rate is several orders of magnitude larger than this, so that this process cannot account for the quenching experimentally observed for the case of oxygen, the most paramagnetic gas.

Spontaneous decay from triplet-to-singlet ground states of Ps may take place by magnetic dipole radiation, the lifetime of the triplet

state against this mode of decay being several months (13). Ortho-to-para conversion due to the electromagnetic field of a non-paramagnetic molecule leads to a lifetime of approximately 12 days and 4 days for the reverse process, so that these processes may be neglected (13).

The direct electron exchange process is largely dependent on the magnetic moment of the colliding molecule. On the other hand, direct annihilation of the Ps atom with an electron from the molecule depends upon Ps energy and the polarizability of the molecule (30).

e. Effects of Oxygen on Orthopositronium in Liquids

One would expect de-oxygenation of organic liquids to increase the long lifetime for positron annihilation. It has been reported that oxygen dissolved in liquid gases and adsorbed on some solids interacts with Ps.

Measurements of the quenching of orthopositronium by oxygen in argon gas, liquid argon and liquid nitrogen were carried out by Paul (31). Assuming a simple gas-kinetic picture, the increased annihilation rate λ^* is directly proportional to the number of oxygen molecules n present. Comparison with volume rates of oxygen was used for the liquids. Ferrell (20) proposed an electron exchange mechanism which is insufficient to explain the results of the strong dependence of temperature on volume rates at low temperatures (around 80°K). The formation of the chemical compound $(e^+e^-)O_2$ was then proposed and presumably applies to liquids. The reaction may be written in the form

$$(e^+e^-) + O_2 + X \longrightarrow (e^+e^-)O_2 + X \qquad (28)$$

which probably describes every collision of Ps atoms and O_2 in liquids.

An exponential fit to the data was observed in which

$$\frac{\lambda^*}{n} = A + Be^{-\Phi/kT} \qquad (29)$$

where the term **A** arises from the electron exchange mechanism, which is perhaps temperature independent. The second term expresses the exponential dependence of λ on temperature.

Lee and Celitans (32) assumed that oxygen quenching of Ps follows second order kinetics, described by the equation:

$$\lambda = \lambda_o + \lambda_q \left[O_2\right] \qquad (30)$$

where λ_q is the quenching constant, λ^{-1} is the observed lifetime at $\left[O_2\right]$ concentration and λ_o^{-1} is the observed long lifetime for the degassed liquid. In their work on several organic liquids, the rate of quenching has been observed to be controlled by the rate of diffusion of oxygen. Either Ps diffuses with thermal velocity or Ps is trapped in the liquid. The increase in annihilation rate was attributed to triplet-to-singlet conversion caused by the oxygen molecule.

Kerr *et al.* (33) determined the intensity of the low-momentum component $I_L = I_2/3$ from angular correlation studies of the annihilation radiation in hexane and degassed hexane. Contrary to the results of Lee and Celitans (32), they conclude that the ortho-to-para conversion is not responsible for the quenching of the positron long lifetime in hexane, since if this were the process responsible, an enhancement of the low-component momentum would be observed. Within limits of experimental error, degassing the samples showed no variation in independent measurement of I_2 and I_L by different detection methods.

Positron Annihilation in Metals

Early experiments on lifetime measurements using delayed-coincidence methods showed the constancy of τ_1 in the different metals studied (1.5×10^{-10} sec.) to within 25 percent (34). Using better time resolution, Bell and Jørgensen (35) reported considerable variation of τ_1 in aluminum and several alkali metals, although the previous result is still presumed to apply to most metals. On the basis of the free electron theory angular correlation data predicted longer lifetimes and annihilation rates proportional to the conduction electron density. Calculated lifetimes using Equation (14) are too long if Coulomb effects are neglected. Allowing Coulomb interaction, Ferrell (20) obtained an annihilation rate nearly independent of velocity, predicting a lifetime in agreement with observation for metals of high conduction electron density, but too low for the lower electron density metals.

The electron momentum distribution from angular correlation data exhibits a maximum at the Fermi cutoff. The higher momentum component is attributed to ion core effects, since the positron wavefunction is excluded from the interior of the ion cores by Coulomb repulsion. The lower component is interpreted to be due to an annihilation probability which is not too strongly velocity dependent.

An exact theoretical treatment of positron annihilation in metals requires the methods of many-body theory, taking into account electron-positron correlation, electron-electron forces and the Pauli principle. Involved computational difficulties introduced by the lattice are encountered, so that certain approximations and simple models become necessary.

Using the electron gas model, Kahana (36,37), calculated the electron density at the position of the positron, taking into account the screening effect (which prevents Ps formation) and the Pauli principle. His results showed the consistency of the Sommerfeld model, treating as accurately as possible positron and metallic valence electron correlation. The variation of annihilation rates with valence electron density in the region of realistic electron densities are in agreement with the experimental results, although the annihilation rates are somewhat too high.

The solution of an extended Bethe-Goldstone equation including both short range positron-electron interaction and short-range positron-electron hole interaction yields positron lifetimes longer than those calculated by Kahana. In metals of low electron densities, plasmon emission which accompanies the two-photon annihilation process may not be neglected (38). This treatment modifies the prediction of angular correlation experiments, since the polarization of the electron plasma by the positron field enhances the effective electron density.

A more rigorous treatment of the problem has been developed (39) in which Bloch wavefunctions are assumed for the positron and conduction band electrons and core electrons are treated within the tight-binding approximation. In this approach, the annihilation rate due to core electrons is proportional to the square of the sum of the Fourier component of the product of positron and core function and a term which accounts for the polarization of the ion core by the positron, which should not be neglected.

Based on the assumption that the Ps state is described by a bound state of the Schrödinger equation, extended theoretical calculations

(40) of the equation of motion for the electron-positron Green's function, approximated by a Schrödinger equation, indicate that quasi-Ps states in metals do not occur with large electron densities. Kanazawa et al. (41) lend support that Ps formation does not occur in the usual range of the density parameter r_s, the radius of a sphere in units of the Bohr radius, a_o, containing on the average one electron.

A weak second lifetime of $\sim 3.0 \times 10^{-9}$ sec. was observed by Bell and Graham (34) which was attributed to the conversion of triplet-to-singlet Ps. The conversion interpretation, however, fails to account for the magnitude of the lifetime. A complex decay was also reported by Bell and Jørgensen (35) which showed that the long lifetime in aluminum accounts for 5 percent of the events. Attempts to show that the tail was due to purely instrumental effects failed. Their data demonstrated conclusively the lifetime dependence on conduction electron density. Kehonen (42), however, has shown that the intensity and slope of the second lifetime is greatly affected by sample preparation techniques. Ideal conditions demand a positron source distributed uniformly throughout the metal to be studied. The Mg metal with Na^{22} produced in situ by the (p,α) reaction provided experimental evidence that the long lifetime is entirely an anomaly of sample preparation involving positrons which come to rest in the region of the surface of the metal or the source itself, and annihilate in areas other than the homogeneous interior of the metal. Ordinarily, positrons are considered to be free, and not bound to any particular valence electron or lattice site (43).

Alkali Halides

Some General Features of Ionic Crystals. A theory of solids should be

able to explain the physical properties of any solid substance as we know them from the atomic structure. The ionic crystals were among the first solids to be treated in this manner, due to the simplicity of their composition. The idealized model of an ionic crystal presupposes that the constituents are positive and negative ions carrying charges distributed with spherical symmetry on each ion, the charges being multiples of the electronic charge. Such compounds are known to crystallize in one of several simple structures (44).

The sodium chloride structure (face-centered) is characteristic of all the alkali halides, with the exception of the low-temperature modifications of CsCl, CsBr, and CsI which are known to crystallize with the simple cubic structure (body-centered). The sodium chloride arrangement allows each atom to have as nearest neighbors six atoms of the opposite kind, and four molecules in a unit cube.

The fluorite lattice is typical of ionic compounds which have the formula A_2X or AX_2. This occurs among the alkaline earth halides, such as CaF_2, SrF_2, BaF_2, and $BaCl_2$ in which the cations are at both the corners and face centers of a cubic unit cell. Eight anions are within this volume, each of which is equidistant from four cations, each cation being surrounded by eight anions.

In the rutile structure, each cation is surrounded by six anions at the corners of an octahedron. In this case, the unit is a parallelepiped rather than a cube. This arrangement is adopted by difluorides and dioxides having smaller cationic radii than those of the fluorite structure. MgF_2, CoF_2, SnO_2, and MnO_2 are examples of ionic crystals which crystallize with the rutile structure (45).

Annihilation in Alkali Halides. The details of the annihilation process in ionic crystals are expected to be quite different from those in metals. The deviation is due to the possible capture of the positron by the halogen ion, so that the Fermi gas model, which applies to most metals, is unsuitable.

a. Positron Lifetimes

One of the first theoretical works on the annihilation of positrons in alkali halides was carried out by Ferrell (20) at which time only the short lifetime had been reported by experimental measurements. Treating the periodic potential problem by the tight binding approximation, he showed that Ps formation in these ionic crystals is not permissible. Since ionic crystals may be considered as closely-packed hard elastic spheres, no room is left to accomodate the Ps atom; the increase in Ps energy due to the "squeezing" of the bound system by the ions in the crystal leads to the depletion of the "Ore-gap". Furthermore, since τ_1 is inversely proportional to the electron density, only the halide ion would play a major part, so that τ_1 would be proportional to the cube of the anion radius. One would then expect significantly increasing positron lifetimes in going from F^- to I^-.

Treating the crystal field of LiH as a sum of central field potentials centered on ion sites, Neamtan and Verall (46) concluded that formation and persistence of the Ps atom in the crystal is energetically favorable. The bound state occurs through the capture of a valence bond electron by the positron. This may then be a possible explanation of the long lifetime in alkali halides reported by Bisi et al. (47,48), in which the decay characteristic shows an empirical regularity within each series. A linear correlation between the decay rate and molecular den-

sity, n, within each halide series was observed, given by the equation

$$\lambda_2 = \lambda_o + Kr^2 n \quad , \tag{31}$$

where λ_o is the extrapolated value (to zero density), $K = 1.90 \times 10^2$ cm sec.$^{-1}$, and r is the anion radius.

Ferrell's conclusion for the non-formation of Ps atoms in ionic crystals is possibly true for perfect specimens of alkali halide crystals. Deviation from perfection due to defects such as vacancies, dislocations and cracks would provide more available space for the Ps, so that its existence and persistence in the crystal should not entirely be ruled out.

A different interpretation of the experimental data has been offered by Gol'danskii et al. (49) in which the positron in Ps annihilates from one of three types of bound states formed in alkali halides through the following processes:

a. capture of positrons by anions at normal lattice sites and the subsequent formation of e^+-anion bound systems with a binding energy of about 1 ev

b. capture of positrons by negative cation vacancies, and also by negative impurities or "host" ions at lattice interstices, with a binding energy of about 1 to 2 ev

c. capture of positrons into Pekar polaron states.

The probability of a two-photon annihilation from polaron states may be calculated from the equation

$$W = \pi r_o^2 c \, \bar{\rho} \tag{32}$$

where $\bar{\rho}$ is the averaged electron density (averaged over the position of

the polaron state of positrons in the crystal), r_o being the classical electron radius. The electron density was chosen to be

$$\bar{\rho} = \sum_i \left| \int \Psi_i^2(\vec{r})\, \chi^2(\vec{r}) d\vec{r} \right| \tag{33}$$

where $\Psi_i(\vec{r})$ is the one-electron Hartree-Fock wavefunctions of anions and $\chi(\vec{r})$ is the positron polaron state wavefunction. This model predicts a positron lifetime of

$$\tau = \frac{1}{W} = 5 \times 10^{-10} \frac{\bar{\rho}_o}{\bar{\rho}} \tag{34}$$

where $\bar{\rho}_o$ is the averaged electron density in a Ps atom given by

$$\bar{\rho}_o = \frac{1}{8\pi a_o^3} \quad . \tag{35}$$

The prompt meanlife is considered to be due to the annihilation of the positron from the 1s polaron state, and the long lifetime is due to annihilation from the 2p polaron state. The theoretically calculated values for τ_1 in the chloride series are larger than experimental results, while the τ_2 appears to agree only in the case of RbCl. The discrepancy between the theoretical and experimental values of both τ_1 and τ_2 has been attributed to the fact that the annihilation of the positron from the polaron state over the entire crystal region occupied by the positron was not taken into account.

b. Angular Correlation Considerations

Since it is natural for the positron to be attracted by the negative ions, it was predicted that the angular distribution of annihilation photons from alkali halides should be determined mainly by the halogen atoms. Furthermore, the width of the distribution should vary with the halide's chemical activity (16). Approximating the positron

wavefunction by a delta-function, in the tight-binding approximation, Ferrell obtained an angular correlation function which is characteristic of the alkali halides. The width of the curve obtained from this function was seen to be inversely proportional to the cube of the Goldschmidt anion radius. These predictions were well confirmed by the measurements of Lang and DeBenedetti (50) on polycrystalline NaCl, KCl, and KI samples and oriented LiF specimens.

Further measurements with single crystal samples of LiF, NaCl, KCl, KBr, and KI were carried out by Millett and Castillo-Bahena (51). They account only for the NaCl data, assuming an overlap wavefunction of the form $(r - b)^2 e^{-mr}$. Their calculations show that best agreement with experimental data occurs when 30 percent of the annihilation events are attributed to s electrons, and the other 70 percent are due to annihilations with p electrons.

Taking the complete sodium halide and alkali chloride series, Stewart and Pope (52) reported that the width criterion alone is not a definitive property of a model. Their calculations based on five different models of positron and electron wavefunctions are incompatible with the assumption that both electrons and positrons may be described by tight-binding wavefunctions. The models which fit the measured momentum distribution have a radial electron distribution similar to that which describes the outer shell electrons of the free ion.

CHAPTER IV

EXPERIMENTAL METHODS

Source and Sample Preparation

The radioactive isotope sodium-22 is the most widely used positron emitter in the laboratory. Its half-life of 2.58 years makes it a more desirable source than copper-64, which has a half-life of 12.9 hours, although this isotope has found some use in some experiments. The positron emitter used in this work was sodium-22. Figure 2 shows the decay characteristics of sodium-22.

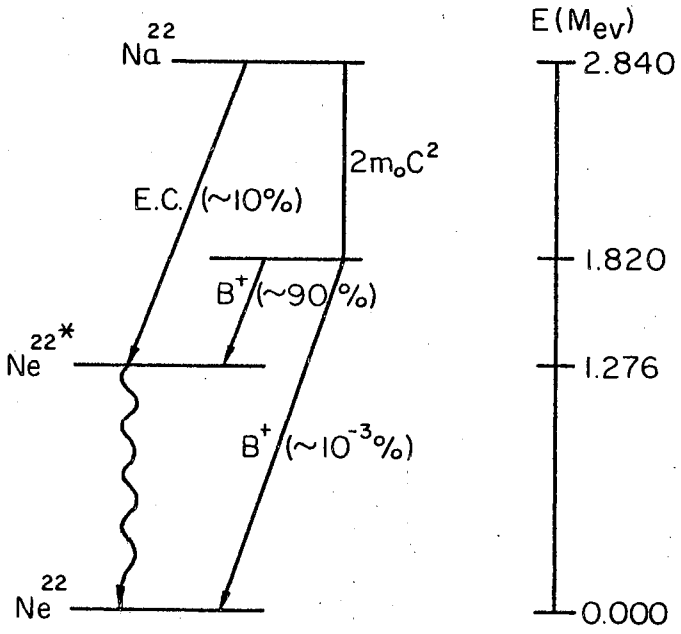

Figure 2. Decay Scheme of Sodium-22

The relations giving the positron decay are:

$$_{11}Na^{22} \longrightarrow + {}_{1}\beta^{\circ} + {}_{10}Ne^{22*} + {}_{o}\bar{\nu}^{\circ}$$

$$_{10}Ne^{22*} \longrightarrow {}_{10}Ne^{22} + \gamma$$

The beta energy spectrum for the sodium-22 isotope yields an endpoint energy of 0.544 Mev.

Fortunately, the transition from the first excited state of neon-22 to the ground state occurs in less than 10^{-11} sec. Since the shortest lifetime observed in this work is 10^{-10} sec., the 1.276 Mev nuclear gamma ray can be taken as emitted simultaneously with the positron.

The sodium-22 nuclide is usually supplied as sodium chloride solution at a specific activity of approximately 0.1 mC/mg NaCl. In this form, the source is readily evaporated on an aluminum or mica sheet and then folded or covered to make a sealed sandwich and inserted in the system under study. The Na^{22} source used in this work was obtained from Nuclear Science and Engineering Corporation. For the lifetime measurements in the fluoride crystals the source was evaporated on household aluminum foil which has a thickness of 0.025 mm., folded and inserted between two identical crystals. All crystals used were single crystals 2.5 cm. in diameter and 0.5 cm. thick (Harshaw Chemical Co., Cleveland, Ohio), so that most of the positrons annihilated in the sample. Household aluminum foil was chosen since it has been especially degreased for household purposes. The crystals were wrapped in electrical tape and positioned between the photomultipliers. A special sample holder was prepared for CsF since this particular crystal is highly hygroscopic.

An almost air-tight glass container was designed which could contain both the sample crystals and dessicant (silica gel and molecular sieve). The portion of the container facing the photomultipliers were microscope slide glasses, which had an average thickness of 0.15 mm. to minimize attenuation of the gamma rays. Trial runs with other crystals with and without this sample holder showed that corrections were unnecessary. Verheijke (53) points out that the eccentric position and finite dimensions of the source affect the efficiency of the scintillators. Since the preparation of the radioactive source described above is far from a point source, precautions were taken in positioning the $Na^{22}Cl$ at approximately the centers of the fluors.

For the alkylbenzenes, glass vials 1.5 cm. in diameter, 4.8 cm. high and a thickness of 1.2 mm. were used to contain the sample. Several milligrams of the organic compound were deposited into the vial and $Na^{22}Cl$ was dissolved into the aqueous solution. A few microcuries are quite enough. Green and Bell (25) have shown that no interaction occurs with NaCl.

The sample preparation for the de-oxygenated alkylbenzenes will be discussed in a separate paragraph, since different containers and source deposition methods were employed. All organic compounds used were of spectroscopic grade supplied by Fisher Scientific Company.

Aluminum and Co^{60} were used as the prompt curves. A few microcuries of $Na^{22}Cl$ were deposited on aluminized mylar foil, evaporated and covered with an identical sheet and mounted on an aluminum retaining ring, 1-3/8 inches in diameter. Aluminum discs 1/10 inch in thickness were mounted on each side of the Na^{22} sandwich. This thickness is sufficient to stop the most energetic positrons emitted by the radio-

active source. The ring fitted snugly over the scintillators used in this experiment. An identical ring was used for the Co^{60} source, which was also deposited on household aluminum foil.

The De-Oxygenation Process

The de-oxygenation technique used is an adaptation of the Hersh technique (54), where the solution is scrubbed with high grade oxygen-free nitrogen bubbles created by a fine dispersion frit. The experimental scheme for the preparation of oxygen-free nitrogen was first devised by Arthur (55). The apparatus used in the preparation of oxygen-free nitrogen in this work was set up by Oeschlager (56) for sample preparation in NMR studies.

Modifications in Oeschlager's assembly in the de-oxygenation of the sample liquid had to be devised to incorporate the freeze-pump-thaw technique. The efficiency of the revised apparatus may be seen from a comparison of the measured values of the relaxation time of chloroform. Oeschlager obtained a relaxation time of 80 sec. at 30°C. A chloroform NMR sample prepared by Melton et al. (57) using the apparatus employed in this work yielded a relaxation time of 85 sec. at 30°C which is in close agreement with the work of Blicharski et al. (58), in which they reported a relaxation time of 95 sec. at 30°C. The latter has been the largest value so far published. Since larger relaxation times of chloroform in NMR studies imply more effective de-oxygenation, the author feels that the revised apparatus described in paragraph B below has a very high efficiency.

A. Preparation of Oxygen-Free Nitrogen. The process and construction of the apparatus are discussed in detail by Arthur (55) and Oeschlager

(56); hence, only a brief outline will be presented below. The chromic-chromous reaction was employed, in which chromic sulfate is reduced by amalgamated zinc. The contrast between the transparent blue color of the chromous solution and the dark green color of the chromic solution renders apparent the condition of the solution.

The important equations of the reactions of these substances are:

$$Zn(Hg) + 2Cr^{+3} \longrightarrow Zn^{+2} + 2Cr^{+2} + Hg$$

$$4Cr^{+2} + O_2 + 4H_3O^{+} \longrightarrow 4Cr^{+3} + 6H_2O$$

while the principal side reactions are:

$$2Cr^{+2} + 2H_3O^{+} \longrightarrow 2Cr^{+3} + 2H_2O + H_2$$

$$Zn + 2H_3O^{+} \longrightarrow Zn^{+2} + 2H_2O + H_2$$

The small amount of hydrogen introduced by this reaction into the gas is harmless in this application since the system is evacuated.

The experimental assembly (56) is presented in Figure 3. Nitrogen gas passes, in order, through a safety trap, A, a scrubber, B, a second safety trap, A', and a second scrubber, B', then through a spray trap, E, and finally a drying trap, F.

Parts C and C' are storage bulbs for the acid-chromium solution when the apparatus is put in stand-by condition. Part D is a pressure relief valve filled with mercury to a depth of 35 to 40 mm., and a loose cotton plug to prevent spattering mercury from getting to the vertical tube K. The spray trap, F, was filled with silica gel in which was also inserted wads of glass wool at the top and bottom to keep the drying agent in place.

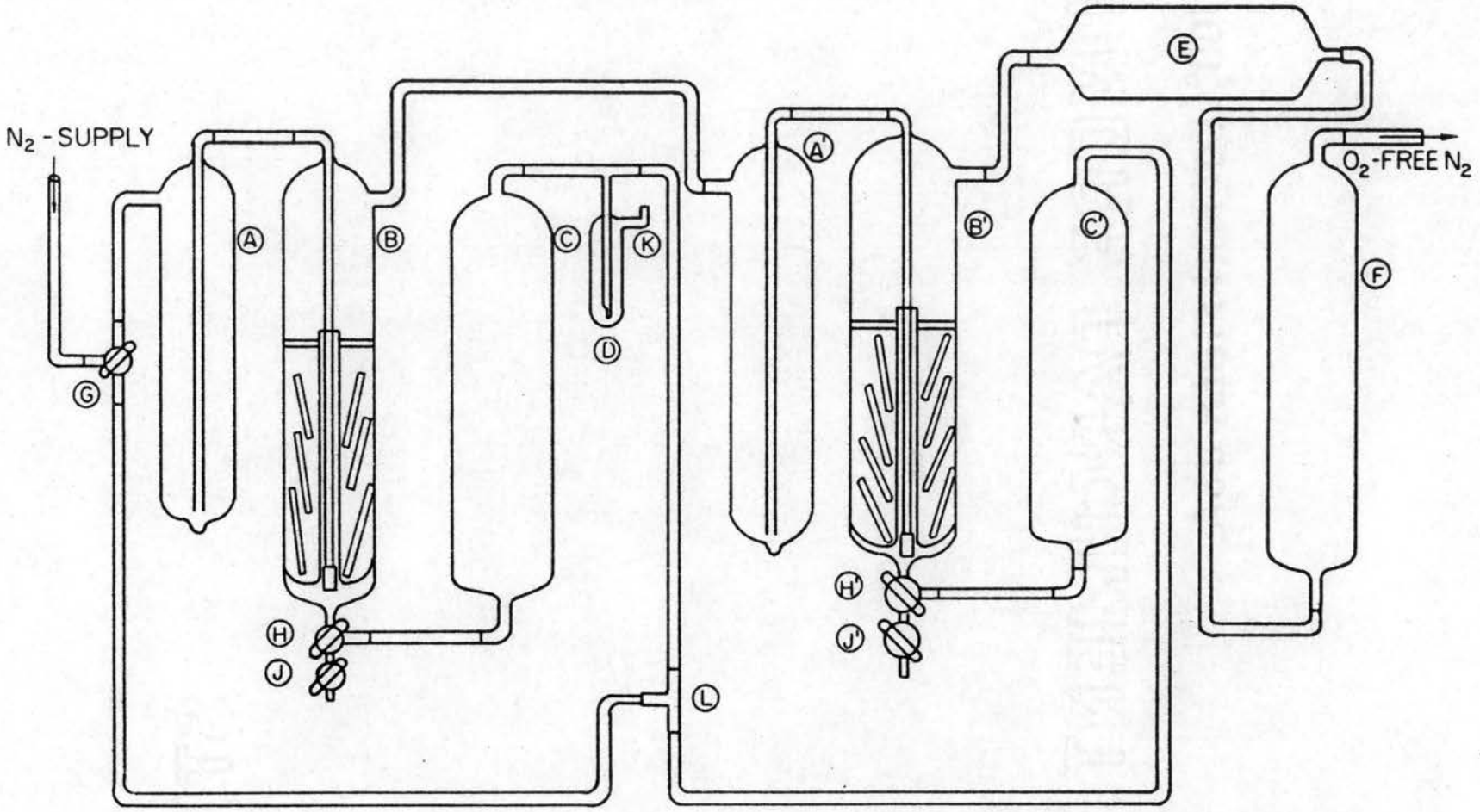

Figure 3. Assembly for the Preparation of Oxygen-Free Nitrogen

All standard joints were fastened using stopcock grease and wire clamps were used to keep the joints from parting under gas pressure. Connective tubings used were 3/16 inch I.D. Tygon tubing.

B. Preparation of De-Oxygenated Positron Annihilation Samples. The de-oxygenation apparatus is shown in Figure 4. This is a revision of Oeschlager's apparatus (56) which was built primarily for large samples. The present design was made for both large and small samples and was constructed to be completely air-tight. All connective tubings were pyrex glass tubings fused to the vessel proper to ensure good vacuum seals. Stopcocks S_1, S_2, S_3, S_4, and S_5 were vacuum leak-proof stop-cocks, and V_1, V_2, and V_3 were low-pressure easy-passing vacuum stop-cocks. Vacuum grease was used to lubricate the stopcocks and each stop-cock was carefully fitted into its proper socket in such a manner so as to remove possible air bubbles caught in the grease. The apparatus consists of four main parts: the sample bottle, P, the de-oxygenation scrubber, Q, the manometer, R, and the trap, T.

The liquid to be de-oxygenated was poured into Q, which was equipped with a fine dispersion frit to provide maximum surface area contact of the liquid with the nitrogen bubbles. The vessel was 2½ inches in diameter, 8 inches high, designed for both large NMR samples and small positron annihilation samples. The vessel was immersed in a Dewar flask packed with salt and ice, throughout the scrubbing process. Lowering the temperature of the liquid decreases the rate of evaporation. In this work, the liquid level should be approximately an inch from the top of the frit. It is important that the entire frit be submerged in the liquid. The stated level provides an allowance for possible evapo-ration. The evaporation observed in the compounds of interest was

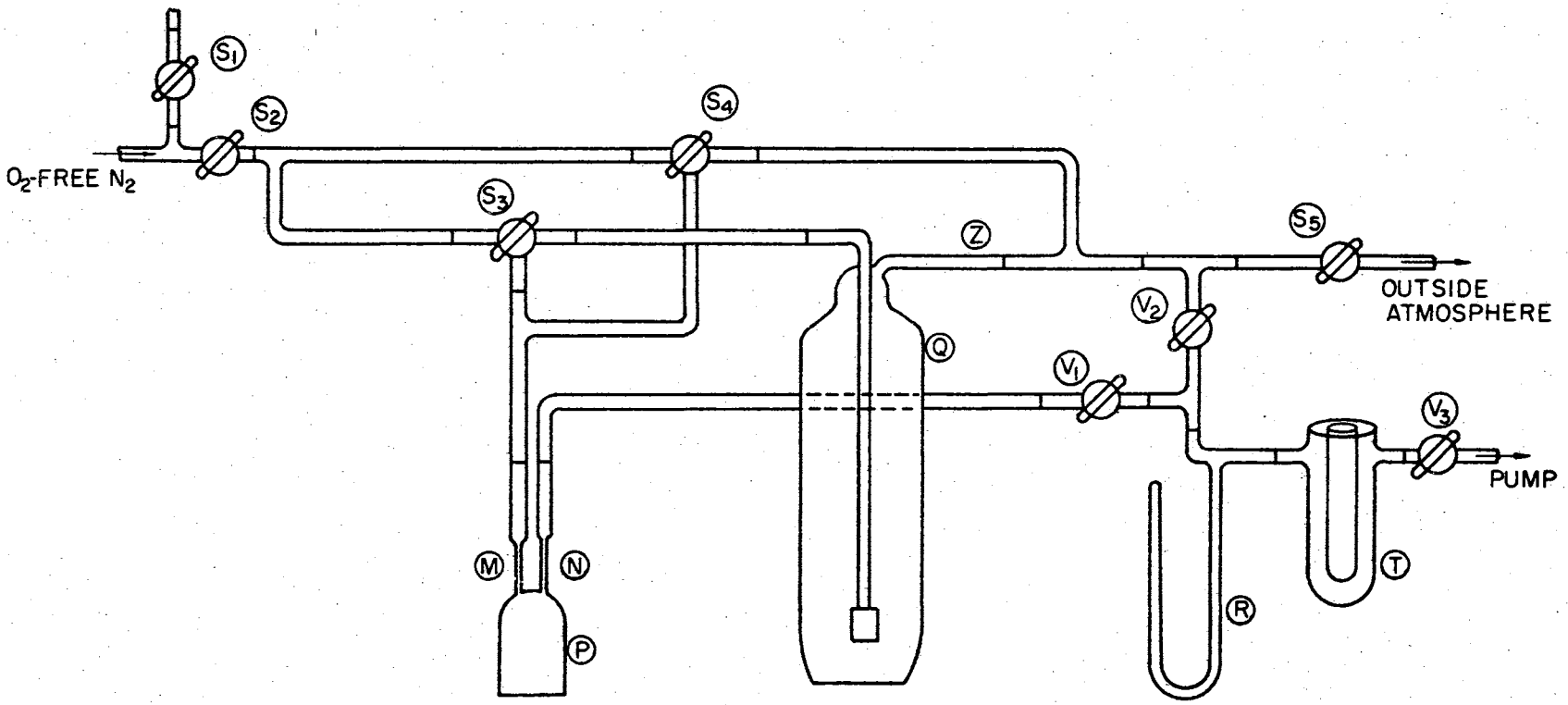

Figure 4. Assembly for the Preparation of De-Oxygenated Positron Annihilation Samples

approximately 1 mm. of the liquid height in Q.

The sample bottle, P, was made of pyrex glass, 5½ cm. high, 2 cm. in diameter, provided with two glass leads, M and N, 1/8 inch in diameter, 3 inches long, fused to pyrex tubings 1/4 inch in diameter to match the leads of the apparatus proper. The radioactive source, Na^{22}, was deposited through M using a disposable plastic syringe. A few drops of distilled water were used to wash down any radioactive material which may have possibly adhered to the inner surface of the tube. The sample bottle was then immersed in a heated oil bath kept at 80°C by means of a Variac, to evaporate the water. Care was taken that the liquid and radioactive source did not boil, to prevent contamination of the leads. After drying, the sample bottle was then connected to the assembly by means of the leads M and N, using a propane torch to melt and fuse the joints. This method required some knowledge of glassblowing.

The oxygen-free nitrogen gas actually flows along two different paths; namely, to de-oxygenate the liquid in Q, and at the same time to continually flush the sample bottle, P. The path along the former leads to a glass tubing, Z, leading to the outside atmosphere via latex tubing, since some of the organic compounds de-oxygenated were poisonous. The latter path allows the continual flushing of the sample bottle throughout the de-oxygenation process. This allowed the flushing and evacuation of the sample bottle several times prior to the transfer of the organic liquid into it.

The U-tube, R, was partially filled with mercury, serving as a manometer. The levels of the mercury in the vertical columns indicated the extent of the vacuum created during the evacuation process.

The U-vessel, T, into which liquid nitrogen was poured during the

pumping process, served as a trap to the vapor-saturated gas. This protected the pump and oil used in evacuating the system.

The de-oxygenation of the liquid was carried out for about 36 hours. At the end of this period, approximately 20 ml. of the liquid in the scrubber, Q, was transferred to the sample bottle by reversing the direction of the nitrogen flow by means of stopcocks S_3 and S_4. Stopcock S_5 closed the system to the atmosphere prior to the transfer. The sample bottle was then flushed with nitrogen to dry all surfaces with which the liquid came in contact. Approximately ten minutes were allowed for drying, after which, stopcock S_2 was turned to stop nitrogen flow into the system.

Liquid nitrogen was used to freeze the liquid in vessel P. As soon as the liquid was frozen, the system was evacuated until the mercury levels in the manometer were equal. Stopcock V_3 was turned to cut off the system from the pump, and the thawing process followed during which the vessel P was immersed in a mixture of tap water and salt. The cycle of the freeze-pump-thaw process was repeated at least four to five times until the frozen sample showed the formation of clear crystals. In that state no opaque gas bubbles were formed and the crystals cracked less easily. Immediately after the final evacuation, the sample bottle was sealed off permanently by fusing the two connecting leads,breaking them away from the equipment proper, while the sample was kept at liquid nitrogen temperature. The sample was then allowed to thaw. In this manner, all chances of an explosion were reduced to a minimum, since at the time of sealing, the sample bottle was still immersed in liquid nitrogen, the system evacuated to a great extent, leaving only about the vapor pressure of the organic solid inside the system.

In effect, the complete process is one of de-oxygenation and de-nitrogenation. It may therefore be referred to as a "degassing" process.

System Arrangement

The delayed coincidence technique is the most widely used method for the measurement of short meanlives. The detection of the 1.276 Mev nuclear gamma ray provides the "preceding" pulse and the 0.511 Mev annihilation gammas provide us with a "delayed" pulse. The distribution of time delays between the two kinds of pulses give us an exponential form ($e^{-t/\tau}$), modified by any timing uncertainties between the two pulses, in which τ is the desired mean life.

A complete coincidence circuit for two sources of pulses must provide for energy selection for each pulse train as well as for time selection. The "fast-slow" principle, first described by Bell and Petch (59) is now generally used in coincidence assemblies. Energy selection occurs in the slow channels in which pulses are unselected as to time, and a coincidence function on pulses unselected as to amplitude is performed in the fast channels. Events satisfying both criteria in time and energy are selected with a slow coincidence element at the end.

A block diagram of the time sorter circuitry used in this work is illustrated in Figure 5. Gamma rays incident on the detectors produce electronic pulses whose amplitudes correspond to the energies of the incident photons. Two outputs are provided for each detector assembly; the output from one of the last dynodes of the photomultiplier goes into the slow circuitry or energy selection channel, and the output from the photomultiplier anode goes into the fast or time selection channel.

Pulse discrimination is applied in the slow channels. One amplifier

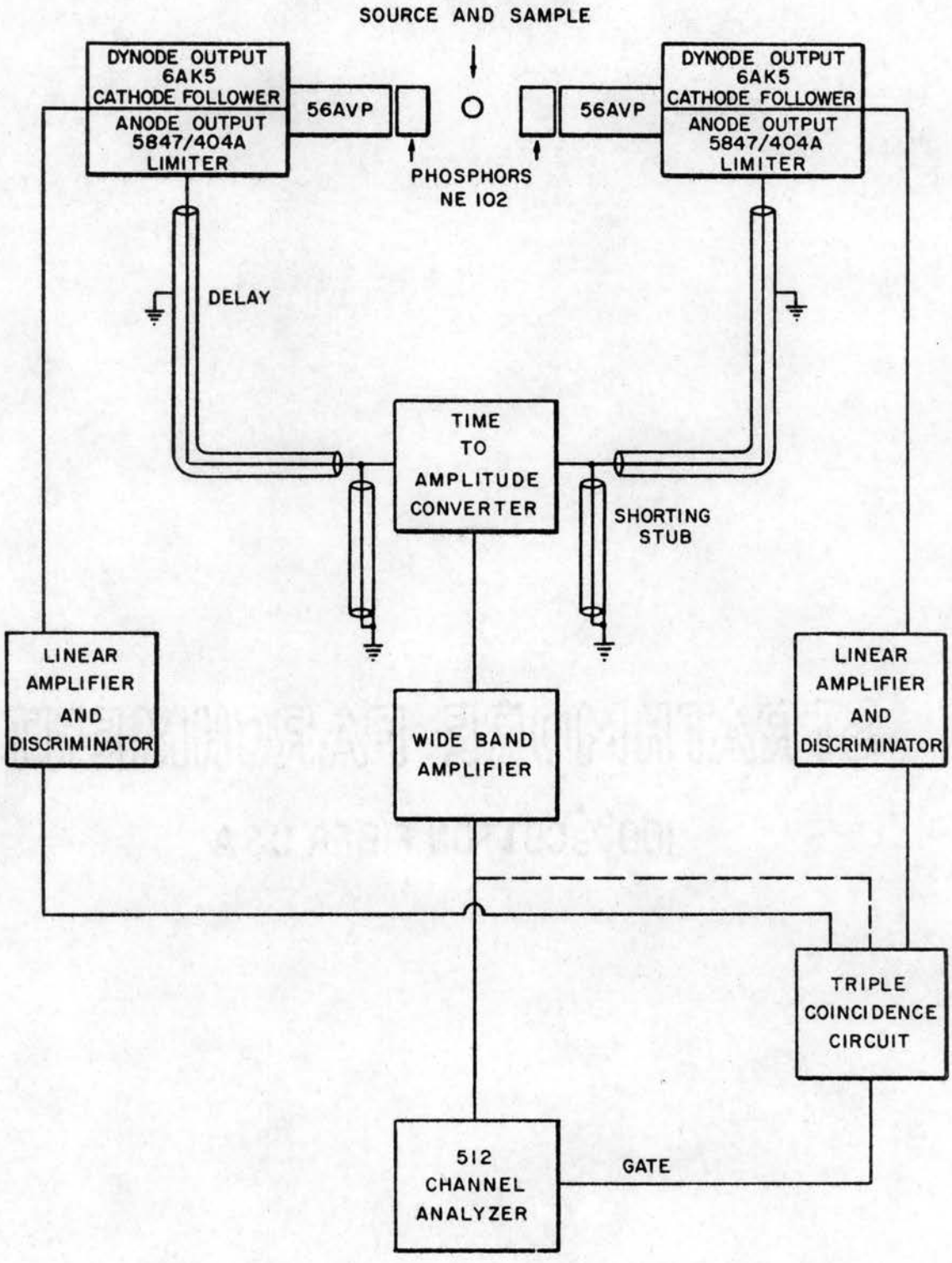

Figure 5. Block Diagram of the Time Sorter Circuitry

is biased to accept only the pulses corresponding to the 1.276 Mev or "creation" quanta, whereas the other is biased to accept both trains of pulses corresponding to the 0.511 Mev or annihilation gamma and 1.276 Mev quanta. The amplifier outputs are then fed into a slow coincidence circuit.

The time pulses are amplified and those with sufficient energy are clipped by a limiter circuit to a step voltage, independent of the gamma ray energy. These are then transmitted to a T-junction at the input of a time-to-amplitude converter by means of coaxial cables. Upon reaching the T-junction, the pulses are clipped to a fixed duration by a shorting stub, so that only the fastest rising pulses are utilized. If a pulse from a second limiter is produced within the activation time of the first limiter, the two waveforms are superimposed at the input of the time-to-amplitude converter. The converter is biased at a particular voltage level, such that only the overlap portion of the waveforms is transmitted to the bias of the integrating circuit. An output pulse is then obtained whose amplitude is proportional to the duration of the overlap.

The output of the slow coincidence circuit in the slow channels is used to gate the multichannel analyzer, so that the analyzer accepts the converter pulses only if both time and energy criteria are satisfied. The analyzer then serves as the second coincidence element.

The entire time spectrum is measured in one observation on the multichannel analyzer. Drifts in the apparatus affect all channels alike, and source decay corrections become trivially easy or wholly unnecessary (60).

Electronic Equipment

DETECTORS.

a. Scintillator

The scintillation phosphors used were NE102 (Nuclear Enterprise, Winnipeg, Canada) organic crystals, 1.5 inches in diameter and one inch long, in thin aluminum covers which fit snugly over the photomultiplier heads. These crystals have a decay constant of 3.5×10^{-9} second. The scintillators were optically coupled head-on to the phototubes with Dow Corning QC-2-0057 silicon grease. Care was taken in getting a good optical coupling since this greatly affects τ_2 and I_2 (61).

b. Photomultiplier

High gain and short transit time required for this work were obtained by the use of the fourteen stage AMPEREX 56AVP photomultiplier tubes. The phototube 56AVP is constructed with a plane and polyoptical window for simplifying and improving the optical coupling of scintillator and photocathode. It has a gain $\geq 10^8$ at 2000 volts, and a spectral sensitivity peaked around 4200 Å. The cathode time difference is 3×10^{-10} second, and the anode pulse is characterized by a rise time of 2×10^{-9} second, at a high voltage of 2000 volts.

The photomultipliers were horizontally positioned 180 degrees to each other. One was socketed in a fixed chassis, the other in an identical chassis which could slide back and forth along rails to facilitate sample changing.

c. Limiter

Each detector chassis was provided with a limiter circuit and

a cathode follower circuit. The limiters used were Amperex 5847 pentodes. The limiter input was obtained from the photomultiplier anode, and the output pulses had fast rising edges, followed by a flat plateau of ~6 microseconds, terminated by a slow exponential decay to zero.

d. Cathode Follower

A simple cathode follower circuit using 6AK5 pentodes proved to be a satisfactory preamplifier for the slow channels. The input was taken from the tenth photomultiplier dynode. The output was cabled to the amplifier input mode by RG-7/U coaxial cables.

TIME-TO-AMPLITUDE CONVERTER.

Delay lines transmitting the limiter pulses to a T-junction at the time-to-amplitude converter input were RG-7/U coaxial cables which have a nominal impedance of 100 ohms. The time pulses were then clipped to a duration of $2t \sim 18 \times 10^{-9}$ second by identical shorting stubs of RG-8/U coaxial cables, 183 cm. in length. The converter inputs were therefore only the fastest rising limiter pulses.

A copy of the time-to-amplitude converter designed by Simms (62) was used, which consisted of two fast switching transistors (T_1 and T_2) followed by a third integrating transistor (T_3). When pulse trains from the two limiters overlap, T_1 and T_2 are cut off, and the current is switched into T_3, where it is integrated at the collector of this transistor. The amplitude of the output pulse is

$$V = \frac{I \Delta t}{C_s}$$

where Δt is the time of pulse overlap and C_s is the stray capacitance. A complete schematic diagram is shown in Figure 6.

Simms recommends Western Electric 2N1195 transistors for short

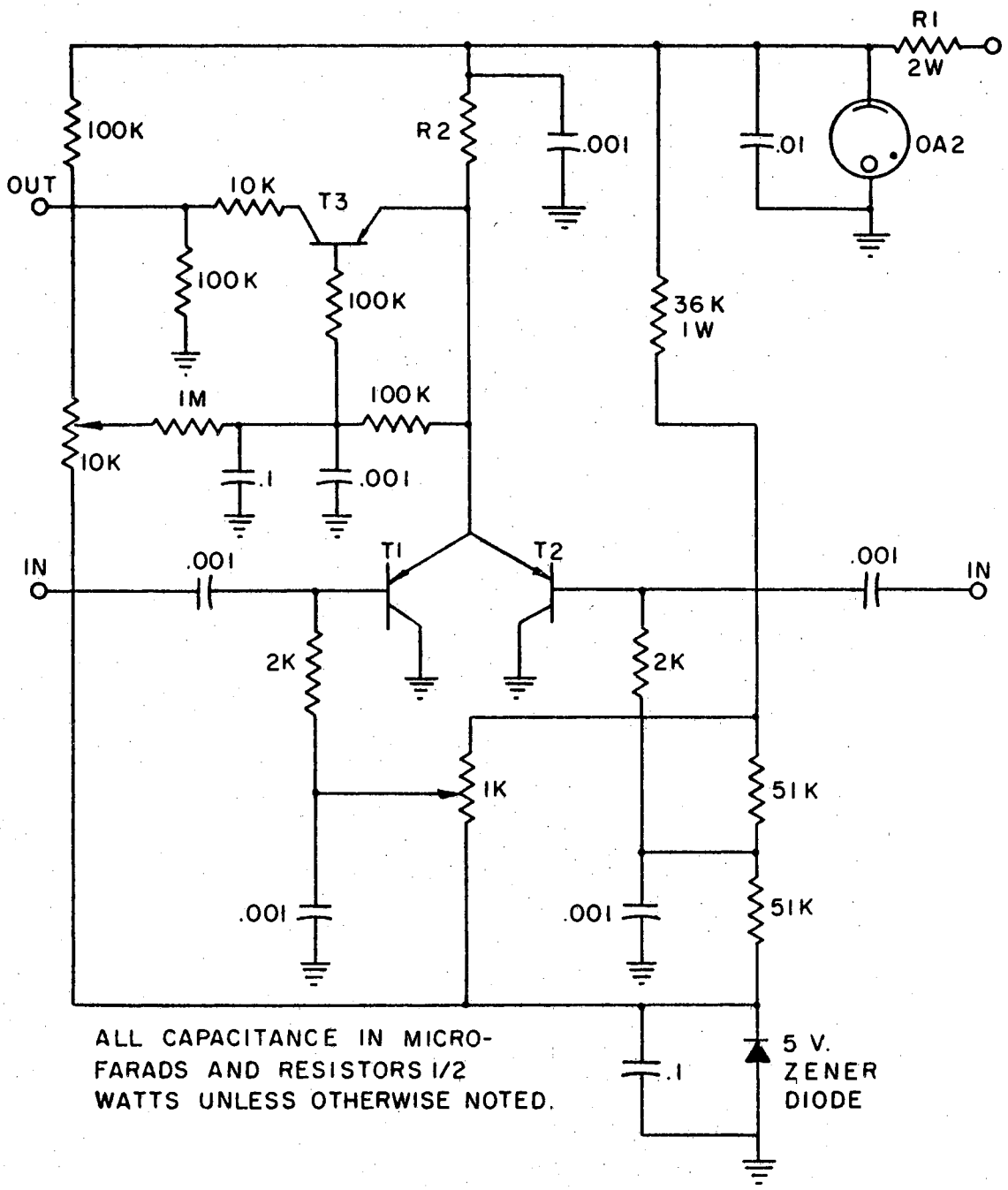

Figure 6. Circuit Diagram of the Time-to-Amplitude Converter (62)

lifetime measurements and Philco 2N501 transistors for regular coincidence experiments. A larger output pulse, may be obtained, resulting in a larger common emitter current. Philco 2N501A were recommended to handle the additional power dissipation safely.

Philco 2N501A transistors were adequate for positron lifetime measurements in the organic compounds. Data collection was also carried out with Western Electric 2N1195 transistors with no appreciable difference.

AMPLIFIERS.

a. Pulse Amplifier

Simm's time-to-amplitude converter gives a positive pulse output which is directly proportional to the time duration of pulse overlap. The detector input mode of the analyzer, which utilizes internal amplification admits only negative pulses. It is then necessary to invert the converter output with no appreciable pulse height loss. A Hewlett Packard Model 460 BR fast pulse amplifier was employed (Hewlett Packard Co., Palo Alto, California) for pulse inversion, so that the analyzer input would be of the right polarity. The fast pulse amplifier is characterized by a rise time of approximately 3 nanoseconds with no appreciable overshoot, and a linear amplifier rated at an output of approximately 8 volts peak into a 200 ohm load or 16 volts peak into open circuit.

b. Coincidence Circuit Amplifiers

Since pulses in the energy channels are unselected as to time, the main concern with the amplifiers used in the slow circuitry was high gain rather than fast rise time. Baird Atomic Model 215 non-overloading amplifiers were used (Baird Atomic, Cambridge, Massachussetts). These

amplifiers have a minimum gain of 72 and a maximum gain of 6,400, a rise time of 0.2 microseconds, and a linearity of 0.5 percent. At maximum gain, the white (random) noise and 60 cps ripple are both 0.5 volts rms.

TRIPLE COINCIDENCE CIRCUIT.

The slow coincidence circuit used in the energy channels was patterned after the Coincidence-Anticoincidence Analyzer Model 401 (Advance Radiation Engineering Corporation, Garland, Texas). A front panel switch allowed for the selection of two or three channel logic modes. The resolving time can be varied continuously from 0.5 to 20 microseconds. The recovery time is 12 microseconds within channels and at the output. A 5 microsecond rectangular pulse, either positive or negative, with an amplitude adjustable from zero to 25 volts is obtained at the output.

MULTICHANNEL ANALYZER.

A Nuclear Data Model ND 130 multichannel analyzer was used for data accumulation (Nuclear Data, Inc., Madison, Wisconsin). This analyzer has a maximum of 512 channels, and is provided with a Tektronix Type RM 503 oscilloscope which displays the time distribution curve stored in the memory core. The time pulses are cabled into the detector input mode, and the slow coincidence output was transmitted to the coincidence input mode, which was used to gate the analyzer.

Data were collected in the lower 256 channels of the analyzer, which was run at an internal gain of 1.0. The time sorter was run on coincidence, which provided the second double coincidence in the circuit. The analyzer output was recorded on an IBM typewriter, which was electronically connected directly to the analyzer.

POWER SUPPLIES.

a. Voltage Regulator

The AC line voltage for the entire system was regulated by a Sorensen Voltage Regulator Model 2000S (Sorensen and Company, Inc., S. Norwalk, Conn.). This instrument has a regulation accuracy of 0.1 percent against line or load at the nominal input frequency (factory-centered at 50 cps) with a resistive load and a time constant of 0.2 second.

b. High Voltage Power Supply

The photomultiplier tubes were operated at 1850 volts, supplied by a Hamner High Voltage Power Supply Model N-4035 (Hamner Electronics Co., Inc., Princeton, New Jersey). This model was designed for applications requiring very high voltage stability, low ripple and sufficient current output for operating several phototubes in parallel. This power supply has a regulation accuracy of 0.005 percent against line between 105 to 125 volts, and 0.005 percent against load between zero to 25 milliamperes. Noise and ripple are less than one millivolt rms.

c. Regulated Power Supplies

The limiters and cathode followers were operated by a Heathkit Regulated Power Supply Model PS-4 (Heath Company, Benton Harbor, Michigan). The positive voltage regulation has an output variation less than 1 percent from no load to full load for outputs of 100 to 400 volts, and a ripple less than 10 millivolts rms. The limiters and cathode followers were operated at 150 volts. An identical power supply was used to operate the time-to-amplitude converter. Since the converter was operated with an independent power supply, the OAS tube

given in Simms' circuit (62) was replaced with a 6AK5 pentode operated at 150 volts.

Calibration of the Time-To-Amplitude Converter

The method of calibration used in this work required the insertion of measured lengths of cable in one or the other side of the fast coincidence circuit and the measurement of the resulting shift of a prompt time spectrum. Systematic errors are involved in this technique, since the velocity of the pulses in the cables are constant only within 5 percent (63).

Aluminum was used as the prompt curve for the alkylbenzenes and RG-7/U coaxial cables with a nominal impedance of 100 ohms were used to delay the time pulses in the 0.511 Mev channel. The channel number of the peak of the prompt curve was plotted against delay, and a least squares fit was used to obtain the slope of the linear region of the resulting curve. The calibration constant was obtained from the slope and the pulse velocity in the cable.

The calibration curve was seen to flatten out at both the tail and at the peak. Data must be collected only in the linear region. All pertinent data collected in this experiment show that no tails extended into the nonlinear region.

With counter biases unchanged, Co^{60} was run with different cable lengths. The calibration constant determined using this source was not too different from that of the aluminum. It was observed, that the difference in the value obtained was less than 3 percent, which is within the limits of error encountered for this method of calibration. Co^{60} was used as the prompt curve for the ionic crystals in this experi-

ment.

Collection of Data

The electronic equipment was tested for performance by using four organic samples (toluene, m-o-p xylenes) of reported positron lifetimes. The experimental results (64) in these samples were in agreement with previously published results (65), within statistical errors.

The ionic crystals were run at resolutions of ~ 0.8 nanosecond as determined from the width at half-height of the Co^{60} prompt curves. The worst resolutions used in this work were in the de-oxygenated alkyl-benzenes runs, in which the resolutions of the aluminum prompt curves corresponded to ~ 1.4 nanoseconds and ~ 1.7 nanoseconds. Since the anomalous lifetime of the positron in the latter compounds was ~ 2.6 nanoseconds, the lifetimes of interest are still well within the over-all resolving time of the electronic system.

Since the calibration of the time-to-amplitude converter is subject to systematic errors, the calibration was repeated several times, and the average value of these runs was used in the lifetime calculations. It was found that the calibration remained constant for many days. The system was re-calibrated each time it was found necessary to turn off the power or a "breakdown" in one of the components occurred.

Data accumulation was carried out until a well-defined time spectrum (composite curve) was observed as viewed on the analyzer oscilloscope. Usually, this corresponded to a peak of ~ 10^4 counts. In all measurements, a minimum of a thousand counts at the peak were recorded before the data were read out on the typewriter. Accumulation time differed from one sample to another due to slight differences in

source strengths.

Immediately before or after each sample run, an aluminum curve was taken for the alkylbenzenes, Co^{60} being used in the case of the ionic crystals. This eliminated timing uncertainties in determining the true zero due to possible instrumental shifts.

In determining the background, data were allowed to accumulate for several hours with the "sample out" for the same time delay used with the sample runs. A few counts were observed in the first ten channels of the analyzer, no counts being recorded in the upper channels. Using a longer delay gave the same result. The background obtained by this method refers to the unwanted coincidences due to the surroundings (i.e., cosmic rays and/or laboratory). Since no portion of the time spectrum of the samples ever fell within the first ten channels, the background referred to above may be neglected. False 0.51 Mev - 1.28 Mev coincidences are neglected, since the time-to-amplitude converter gives a high doubles to singles ratio (62).

However, another source of background comes from the interdetector scattering of photons due to the detector geometry used in this work. Scattering would occur more frequently with higher energy photons which correspond to coincidences recorded in the upper channels. Since this gives a more representative measure of background, the counts in the uppermost channels (usually 10, as determined by the "trailing" off of the spectrum) were averaged, and this value was subtracted from each of the points on the composite curve. A peak to background ratio of 10^4:1 was attained with the alkylbenzenes and ionic crystals, and a ratio of 10^3:1 for the de-oxygenated organic samples.

At least twenty runs were carried out for each of the ionic crystals

and alkylbenzenes. Each of the de-oxygenated samples was run at least ten times. Since the alkylbenzenes chosen reacted with light, the bottles were wrapped in black tape and care was taken that data be accumulated shortly after de-oxygenation.

CHAPTER V

DATA REDUCTION AND PRESENTATION

Analysis of Data

The centroid shift technique introduced by Bay (66) is subject to systematic errors such as drifts in photomultiplier transit time and changes in pulse size distribution (43). The slope method was used in this work, which is insensitive to small changes of this kind. Since a high peak-to-background ratio would eliminate some uncertainties in the latter method having obtained a ratio of 10^4:1, the author felt that the slope method is a more reliable method of analysis.

Two lifetimes were observed in all the measurements performed. The curves were plotted on semi-log paper and the linear "tail" was visually determined. After correcting for background, a straight line was fitted by the least squares method (67). The slope of this "tail" and the calibration constant, K, determines the mean lifetime of the positron in the material, given by the equation

$$\tau_2 = \frac{K}{\text{Slope}} \tag{36}$$

In calculating for the intensity of I_2, the true zero of the time spectrum is necessary. The true zero was determined from the centroid of the "prompt" curve corresponding to each sample run. A Gaussian curve ,

$$y(x) = y(x_o)\, e^{-(x - x_o)^2/2\sigma^2} \qquad (37)$$

was fitted by the least squares technique to the prompt curve, P(x). For each value of x (channel number) of P(x), the ratio of the number of counts corresponding to the preceding channel (x - 1) and subsequent channel (x + 1) was determined. The natural logarithm of such ratios was calculated for the different channels and for a perfect Gaussian distribution, the plot of these ratios versus channel number would yield a straight line (68). Due to the detector response to photon energies, the prompt curve would be semi-Gaussian, which is easily seen from the deviation of the empirical points from a straight line. The x-intercept of the "best" straight line after a least squares fit determines the centroid of P(x). (See Appendix A). Following the methods of Bell and Jørgensen (35) and Green and Bell (25) the centroid of the prompt curve obtained by replacing the positron sample with a Co^{60} source with the same counter settings, determined the true zero for the ionic crystals. In the case of the organic compounds the centroid of the aluminum prompt curve corrected for the positron lifetime in aluminum determined the zero of delay. The positron lifetime value in aluminum used in this work is $\tau_{Al} = 1.9 \times 10^{-10}$ second (35).

The linear tail which determines the long lifetime was then extrapolated back to the true zero of the delayed coincidence curve. The value of I_2 may be approximated by the area under this straight line to the right of the zero position, divided by the total area under the curve. A correction factor given by

$$\frac{\tau_o}{\tau_2}\left[\sinh \frac{\tau_o}{\tau_2}\right]^{-1} \qquad (38)$$

where τ_o is the half-width at half-height of the prompt resolution curve, is required due to the finite width of the prompt curve.

The presence of a valley on the left portion of the spectrum prevented accurate calculations of the total area under the curve. Since large errors are usually associated with I_2, the left-hand portion of the curve was extrapolated, following the general shape of the prompt curve.

The determination of the short lifetime τ_1 was obtained by subtraction of the τ_2-component from the composite curve. A straight line was fitted to these resulting points using the least squares method, identical to that used in determining τ_2.

In this analysis, τ_1, τ_2, and I_2 were allowed to vary. Computer programs were written for all the calculations carried out: the least squares method for the determination of the calibration constant, true zero or centroid, τ_1 and τ_2, and Simpson's rule for determining I_2. All calculations were carried out on the IBM 7040 digital computer.

The effects of the ratio of the cation radius to the anion radius and interionic distance upon τ_1, τ_2, and I_2 were calculated by a stepwise regression analysis. This analytic method is based on the "Doolittle Method" (69), assuming a model of the form

$$Y = a_o + a_1X_1 + a_2X_2 + \ldots + a_nX_n \qquad (39)$$

where X_1, X_2, . . . X_n are independent variables which affect Y as determined by the so-called "F" variate.

The "F" variate is a statistical distribution, which is the ratio of two chi-square variates, each divided by its respective degrees of freedom. The stepwise operation allows the independent variables to enter the regression equation in the order of decreasing effect on Y.

Elimination of the parameters which hardly have any effect on the dependent variable is done at a predetermined F-level. That is, only those variables for which the F-values as given by the ratio of the regression mean square to the error mean square are greater than the predetermined F-level (0.001 in this work) are included in the final regression equation.

The influence of any independent variable on the dependent variable may be seen from the magnitude of its F-level; a larger value implies a larger effect, adjusted with respect to the coefficients of the preceding parameters. A comparison of the calculated F-variate, with known degrees of freedom, with the cumulative distribution tables (69) gives the probability of committing a "Type I error", which is the error involved in rejecting a hypothesis that is true. It should be noted that the criterion for the closeness of fit should not be the difference between the experimental and the calculated values, but rather, the magnitude of the error probability.

Presentation and Interpretation of Results

Alkylbenzenes. Tables I and II show the results of this work on the alkylbenzenes. The normal state of the samples will be referred to as the "oxygenated" group to distinguish these samples from the "de-oxygenated" class. The word "oxygenated" might be misleading, but all that is meant by the use of the term is the state of the sample which contains the normal amount of oxygen present at ordinary conditions. The errors quoted are at least twice the statistical errors obtained.

A very striking feature of the results shown in Table I is the constancy of the long lifetime. It is plausible that the presence of

the paramagnetic oxygen molecules in these samples masks the contribution from the alkylbenzenes. The rapid quenching may be attributed to the formation of the complex $(e^{+}e^{-})O_2$, which was first suggested by Paul (31).

TABLE I

EXPERIMENTAL RESULTS IN THE OXYGENATED ALKYLBENZENES

	$\tau_1 \times 10^{10}$ sec.	$\tau_2 \times 10^{9}$ sec.	I_2(%)
Isopropylbenzene	5.78 ± 0.28	1.91 ± 0.06	70 ± 3
n-Butylbenzene	4.31 ± 0.12	1.92 ± 0.16	67 ± 2
iso-Butylbenzene	4.15 ± 0.12	1.92 ± 0.16	68 ± 2
sec-Butylbenzene	4.16 ± 0.16	1.90 ± 0.24	67 ± 2
tert-Butylbenzene	4.05 ± 0.14	1.88 ± 0.14	66 ± 2

TABLE II

EXPERIMENTAL RESULTS IN THE DE-OXYGENATED ALKYLBENZENES

	$\tau_1 \times 10^{10}$ sec.	$\tau_2 \times 10^{9}$ sec.	I_2(%)
Isopropylbenzene	5.53 ± 0.20	2.62 ± 0.05	64 ± 2
n-Butylbenzene	6.37 ± 0.18	2.83 ± 0.04	63 ± 4
iso-Butylbenzene	6.29 ± 0.14	2.72 ± 0.04	69 ± 2
sec-Butylbenzene	6.90 ± 0.14	3.26 ± 0.06	64 ± 3
tert-Butylbenzene	6.72 ± 0.10	2.98 ± 0.06	64 ± 2

Considering the intensity of the long lifetime, it is seen that the majority of the annihilating positrons form bound states prior to annihilation. Approximately 2/3 of all positrons participating in the decay process form orthopositronium, whereas approximately 22 percent form parapositronium, leaving about 12 percent to annihilate from the free state. The slight decrease in I_2 upon de-oxygenation is consistent with the results of Kerr *et al.* (33) on hexane.

The results on the de-oxygenated organic liquids are consistent with the electron donating properties of the alkyl branch to the benzene ring by inductive effects. A good measure of this would be the σ^* constants, which are also known as the polar substituent constants. The values of σ^* for the different samples (70) are given in the table below.

TABLE III

σ^* CONSTANTS FOR THE ALKYLBENZENES

	τ_2 (x 10^9 sec.)	σ^*
Isopropylbenzene	2.62	-0.190
n-Butylbenzene	2.83	-0.130
iso-Butylbenzene	2.72	-0.125
sec-Butylbenzene	3.26	-0.210
tert-Butylbenzene	2.98	-0.300

A more negative σ^* value implies a greater electron donating ability of the substituent to the benzene ring. The τ_2 values give evidence that annihilations take place with the electrons of the substituent rather

than with those of the benzene ring, as seen from Table IV.

TABLE IV

POSITRON LIFETIMES VS σ^*

	τ_1(x 10^{10} sec.)	τ_2(x 10^{10} sec.)	σ^*
iso-Butylbenzene	6.29	2.72	-0.125
n-Butylbenzene	6.37	2.83	-0.130
tert-Butylbenzene	6.72	2.98	-0.300

The structures are as follows:

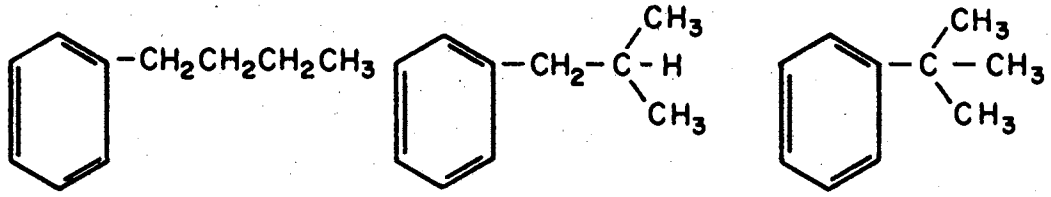

n-BUTYLBENZENE iso-BUTYLBENZENE tert-BUTYLBENZENE

The fact that the positron lifetimes in isopropylbenzene and sec-butylbenzene do not fit in the above analysis may be explained by the formation of hydroperoxides. These two organic compounds are similar in structure as seen from the diagrams on the following page.

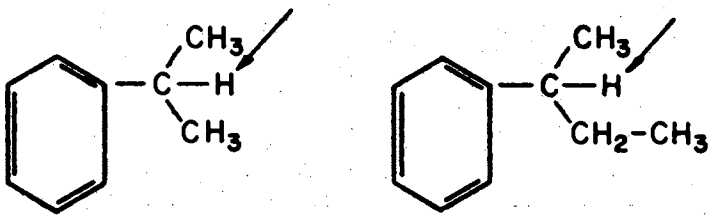

ISOPROPYLBENZENE sec-BUTYLBENZENE

The hydrogen atoms designated by arrows are quite reactive and in the presence of oxygen will form compounds of the: - O - O - H group. The reactions may be written as

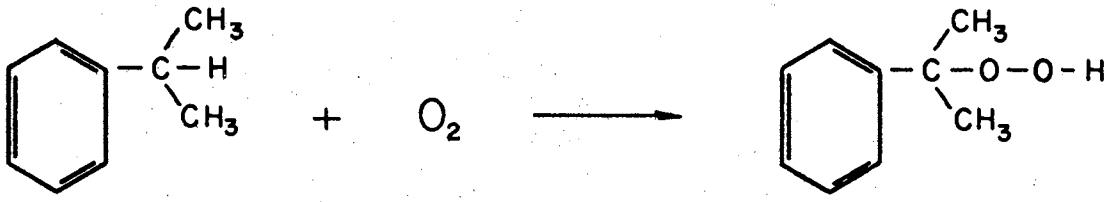

and

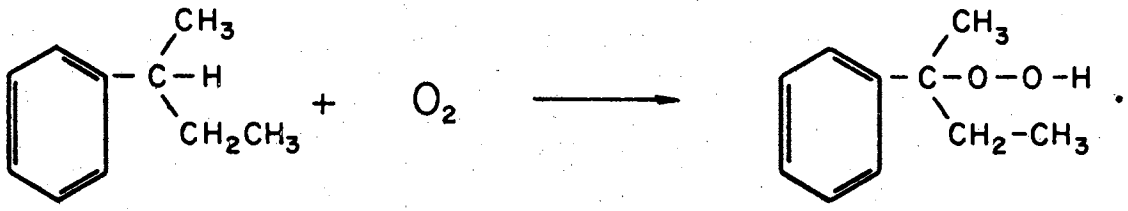

Hydroperoxides most likely were formed, since isopropylbenzene and sec-butylbenzene are non-resistant to this type of oxidation, whereas n-, iso-, tert-butylbenzene are more resistant (71). This oxidation process may be looked upon as a hydration process, in which the water molecules

formed prevent sufficient contact between Ps and electrons of the neighboring molecules. This picture is consistent with the quenching process due to the pickoff mechanism.

In choosing the organic compounds, the interest was in τ_2 rather than in I_2. The results on I_2, however, show that dissolved oxygen has very little effect on the amount of orthopositronium formed. The alkyl substituents are known to effect an increase in the electron density on the ring, so that the group added becomes the positive end of the dipole. Since the negative charge is smeared out over the benzene ring, a less marked effect is expected. Substituents such as the halogens, in fact, affect I_2 greatly, since the negative charge is more concentrated (65). The results also exhibit a very slight dependence of chain length of the alkyl substituent on τ_2.

Alkali Halides. The results on the positron short lifetime, τ_1, in alkali halides in this study are listed in Table V together with previous work. All theoretical calculations make use of the electron density at the position of the positron in terms of the Ps atom as the basis of comparison. Ferrell's (20) model assumes that the electrons are uniformly smeared out over the volume of a sphere of radius a. Only the eight electrons occupying the noble gas configuration are assumed to contribute to the annihilation process, since the inner electrons are more tightly bound and are therefore never sampled by the thermal positrons. The second column lists calculations based on this model, using the Goldschmidt anion radius. The third column is patterned after the same model using corrected anion radii based on x-ray methods (72). Goldanskii et al. (49) report the τ_1 values as determined by positrons annihilating from the 1s polaron state.

TABLE V

COMPARISON OF THE POSITRON SHORT MEANLIFE
$\tau_1 \times 10^{10}$ SEC.

	Theoretical				Experimental		
	Ferrell (73)	Ferrell (73)	Gol'danskii (49)				
	(Goldschmidt r)	(Corrected r)	1s Polaron	Interstitial	Bisi et al. (47)	Pollak (73)	This Work
LiF	1.67	0.92		7.00		1.9 ± 0.2	3.25 ± 0.18
NaF	1.67	1.11	3.6	4.25		2.4 ± 0.2	2.97 ± 0.08
KF	1.67	1.11					3.25 ± 0.06
CsF	1.67	1.11					3.04 ± 0.08
KF	1.67	1.11					3.25 ± 0.06
KCl	4.20	3.15	3.1	2.80	2.2 ± 0.9	3.0 ± 0.2	3.79 ± 0.06
KBr	5.38	4.13				3.4 ± 0.3	4.02 ± 0.14
KI	7.46	6.13				3.9 ± 0.3	3.92 ± 0.10

The measurements for which twice the statistical errors obtained are quoted, are consistent with the hypothesis that the positron prompt meanlife is determined mainly by the halogen ion, although the simple relation between τ_1 and the cube of the anion radius cannot be reconciled. The results on the potassium halide series show an increasing lifetime in going from F^- to I^- except for the case of potassium iodide. The discrepancy may be attributed to the large halide radius, in which case Ferrell's model may not be valid; however, this observation agrees with Pollak (73).

The analytic proof of the τ_1 dependence on the halogen ion may be seen from the results of the regression of cation-anion ratio and interionic distance on τ_1. These are shown in Tables VII through X, where the constants listed in Table VI were used. These constants were used in all the regression analyses for the alkali halides. From the error probabilities listed in Tables VIII and X, one can immediately see that the alkali ion hardly has any effect on τ_1. The anion radius greatly affects τ_1; the analysis shows a square dependence rather than a cubic dependence as predicted by Ferrell (20).

TABLE VI

CATION-ANION RATIOS AND INTERIONIC DISTANCES
OF THE ALKALI HALIDES

	r_+/r_- (74)*	Interionic Distance (75) x 10^8 cm.
LiF	0.5865	2.07
NaF	0.7368	2.31
KF	1.0000	2.66
CsF	1.2556	3.00
KF	1.0000	2.66
KCl	0.7348	3.14
KBr	0.6786	3.29
KI	0.6073	3.53

*The ratios are based on the Goldschmidt ion radii taken from Reference (74) except for the lithium ion for which there seems to have been a typographical error. The value used in this work is 0.78 angstrom, which was obtained from Reference (45).

The regression model for τ_1 in the alkali fluorides is given by the equation

$$\tau_1 = a_o + a_1(r_{int}) + a_2(r_+/r_-) \qquad (40)$$

where $a_o = 10.28750 \times 10^{-10}$ sec.,

$a_1 = -5.51917 \times 10^{-2}$ sec/cm.,

and $a_2 = 7.48063 \times 10^{-10}$ sec.

TABLE VII

REGRESSION MODEL RESULTS FOR τ_1
ALKALI FLUORIDES

	Actual $\times 10^{10}$ sec.	Predicted $\times 10^{10}$ sec.	Deviation
LiF	3.25	3.25022	-0.00022
NaF	2.97	3.04995	-0.07995
KF	3.25	3.08715	0.16285
CsF	3.04	3.12268	-0.08268

TABLE VIII

STATISTICAL LEVELS FOR τ_1 REGRESSION MODEL
ALKALI FLUORIDES

Parameter	F	Error Probability
r_{int}	0.1527	0.741
r_+/r_-	0.4602	0.663

The regression model for τ_1 in the potassium halides is given by the following equation:

$$\tau_1 = b_o + b_1(r_+/r_-)^2 + b_2(r_{int})^2 \qquad (41)$$

where $b_o = 5.77256 \times 10^{-10}$ sec.,

$b_1 = -1.88840 \times 10^{-10}$ sec.,

and $b_2 = -0.09041 \times 10^{6}$ sec/cm.^{2}

TABLE IX

REGRESSION MODEL RESULTS FOR τ_1
POTASSIUM HALIDES

	Actual $\times 10^{10}$ sec.	Predicted $\times 10^{10}$ sec.	Deviation
KF	3.25	3.24448	0.00552
KCl	3.79	3.86158	-0.07158
KBr	4.02	3.92439	0.09561
KI	3.92	3.94955	-0.02955

TABLE X

STATISTICAL LEVELS FOR τ_1 REGRESSION MODEL

Parameter	F	Error Probability
$(r_+/r_-)^2$	29.2404	0.037
$(r_{int})^2$	0.4909	0.654

Table XI lists the comparison on τ_2. With the exception of CsF, the measurements in this work are larger than any of the previous works. A possible explanation may lie in the difference of the crystalline aggregates. Bisi et al. (48) used polycrystalline samples except in the case of KCl. All of the samples used in this work were single crystals This point, however, is inconsistent with the observation of Bisi et al.

(76) in their work on three-photon annihilation. No difference in τ_2 for polycrystalline and single crystal samples of NaCl was noted. However, on the basis of symmetry, in multicrystalline materials the periodicity of the structure is interrupted at grain boundaries. It is plausible that the difference between single crystals and polycrystals is the reasonable explanation for the disagreement on the angular correlation results (51,52) in NaCl and KCl.

TABLE XI

POSITRON ANOMALOUS LIFETIME COMPARISON

	Theoretical	Experimental	
	Gol'danskii et al. (49) x 10^{10} sec.	Bisi et al. (48) x 10^{10} sec.	This Work x 10^{9} sec.
LiF		4.02 ± 0.20	1.68 ± 0.04
NaF	6.25	5.05 ± 0.35	1.96 ± 0.10
KF		6.20 ± 0.40	1.11 ± 0.06
CsF		7.60 ± 0.21	0.84 ± 0.04
KF		6.20 ± 0.40	1.11 ± 0.06
KCl	5.30	6.07 ± 0.12	1.03 ± 0.06
KBr		6.73 ± 0.22	1.55 ± 0.06
KI		6.40 ± 0.21	1.31 ± 0.06

In the case of the alkali fluoride series, a decreasing anomalous lifetime with increasing cation radius was observed whereas the results of Bisi et al. (48) showed the opposite trend. The results can be explained on the basis that a larger cation would effect a greater

Coulomb repulsion on the positron, so that enhancement of the annihilation rate should be observed. In the case of LiF, an "anomaly" was observed. It should be noted, however, that the LiF bond has a greater covalent bond than any other alkali fluoride bond (77). Wallace (12) pointed out that the covalent bond effects a repulsive force, so that an increase in annihilation rate or decrease in lifetime is expected. If this reasoning is valid, τ_2 in LiF would therefore not be an anomaly.

The results of the computerized stepwise regression analysis on τ_2 show a marked dependence on the alkali ion. The mathematical models and results of the calculations are shown in Tables XII through XV. In the case of the fluoride series, a reasonable fit can be obtained when one assumes a square dependence of the long lifetime on cation radius. The interionic distance variable does not seem to have a large effect on τ_2, as evidenced by the large error probabilities.

The regression model for τ_2 in the alkali fluorides is given by the equation

$$\tau_2 = a'_o + a'_1(r_+/r_-)^2 + a'_2(r_{int})^2 \qquad (42)$$

where $a'_o = 7.19470 \times 10^{-10}$ sec.,

$a'_1 = -2.52880 \times 10^{-9}$ sec.,

and $a'_2 = 4.46380 \times 10^{6}$ sec/cm.^{2}

TABLE XII

REGRESSION MODEL RESULTS FOR τ_2
ALKALI FLUORIDES

	Actual x 10^9 sec.	Predicted x 10^9 sec.	Deviation
LiF	1.68	1.76228	-0.08228
NaF	1.96	1.72855	0.23145
KF	1.11	1.34905	-0.23905
CsF	0.84	0.75012	0.08988

TABLE XIII

STATISTICAL LEVELS FOR τ_2 REGRESSION MODEL
ALKALI FLUORIDES

Parameter	F	Error Probability
$(r_+/r_-)^2$	9.1901	0.097
$(r_{int})^2$	0.1241	0.799

The regression model for τ_2 in the potassium halides is given by the equation

$$\tau_2 = b'_o + b'_1(r_{int})^2 + b'_2(r_+/r_-)^2 \qquad (43)$$

where $b'_o = 4.24010 \times 10^{-10}$ sec.,

$b'_1 = 7.31100 \times 10^5$ sec/cm.^{2},

and $b'_2 = 1.53480 \times 10^{-10}$ sec.

TABLE XIV

REGRESSION MODEL RESULTS FOR τ_2
POTASSIUM HALIDES

	Actual $\times 10^9$ sec.	Predicted $\times 10^9$ sec.	Deviation
KF	1.11	1.09476	0.01524
KCl	1.03	1.22767	-0.19767
KBr	1.55	1.28599	0.26401
KI	1.31	1.39158	-0.08158

TABLE XV

STATISTICAL LEVELS FOR τ_2 REGRESSION MODEL
POTASSIUM HALIDES

Parameter	F	Error Probability
$(r_{int})^2$	0.7864	0.484
$(r_+/r_-)^2$	0.0029	~ 1.000

The intensity of the long-lived component is shown in Table XVI. The theoretical result of Gol'danskii et al. (49) and the experimental measurements of Bisi et al. (48) were included for comparison.

TABLE XVI

INTENSITY OF THE ANOMALOUS LIFETIME

	Theoretical (%)	Experimental (%)	
	Gol'danskii et al. (49)	Bisi et al. (48)	This Work
LiF		70 ± 15	43 ± 2
NaF		49 ± 5	34 ± 2
KF		33 ± 7	52 ± 3
CsF		46 ± 5	65 ± 2
KF		33 ± 7	52 ± 3
KCl	35 ± 7	50 ± 15	61 ± 2
KBr		37 ± 7	51 ± 2
KI		43 ± 7	52 ± 2

Considering the potassium halide series, the amount of ortho-Ps formed is approximately 50 percent, independent of the halide ion. The intensity of KCl is somewhat higher than the rest by about 20 percent, which was rather unexpected. The results of Bisi et al. (48) on the potassium halide series give fairly constant I_2 values. It is rather difficult to draw definite conclusions based on their results, since the statistical errors are quite large. It can be seen, however, that their measurements on I_2 for the sodium halide, potassium halide and cesium halide series are more or less constant within each particular halide series. One can therefore conclude that the alkali ion determines the amount of positrons taking part in the annihilation process after formation of triplet bound states. This conclusion is, in fact, sup-

ported by the results of the calculations given in Tables XVII through XX. A square dependence of I_2 on the cation radius gives the minimum error for the regression model as seen from Table XVIII. No meaningful interpretation can be given to the relation between I_2 and interionic distance.

The regression model for I_2 in the alkali fluorides is given by the equation

$$I_2 = a''_o + a''_1(r_+/r_-)^2 + a''_2(r_{int})^2 \qquad (44)$$

where $a''_o = 110.29062$,

$a''_1 = 117.99213$,

and $a''_2 = -25.52147 \times 10^{16}/cm^2$.

TABLE XVII

REGRESSION MODEL RESULTS FOR I_2
ALKALI FLUORIDES

	Actual (%)	Predicted (%)	Deviation
LiF	43	41.52087	1.47913
NaF	34	38.16039	-4.16039
KF	52	47.70304	4.29696
CsF	65	66.61568	-1.61568

TABLE XVIII

STATISTICAL LEVELS FOR I_2 REGRESSION MODEL
ALKALI FLUORIDES

Parameter	F	Error Probability
$(r_+/r_-)^2$	9.4754	0.096
$(r_{int})^2$	1.2553	0.487

The regression model for I_2 in the potassium halides is given by the equation

$$I_2 = b''_o + b''_1(r_+/r_-)^2 + b''_2(r_+/r_-)(r_{int}) \qquad (45)$$

where $b''_o = -564.02910$,

$b''_1 = -269.38794$,

and $b''_2 = 332.88562 \times 10^8/cm$.

TABLE XIX

REGRESSION MODEL RESULTS FOR I_2
POTASSIUM HALIDES

	Actual (%)	Predicted (%)	Deviation
KF	52	52.05872	-0.05872
KCl	61	58.57767	2.42233
KBr	51	55.11675	-4.11675
KI	52	50.24692	1.75308

TABLE XX

STATISTICAL LEVELS FOR I_2 REGRESSION MODEL
POTASSIUM HALIDES

Parameter	F	Error Probability
$(r_+/r_-)^2$	0.0149	~0.900
$(r_+/r_-)(r_{int})$	1.5276	0.470

Alkaline Earth Fluorides. About the only work reported on positron lifetimes in alkaline earth crystals are those on multicrystalline BeO, MgO, CaO, and BaO (78), in which a long lifetime was observed besides the short-lived component. The values of I_2 (1 to 7 percent) observed were larger by a factor up to 15 than that calculated, assuming Ps formation. The experimental results on these oxides lend further support that positron-bound systems can be formed and persist in crystals displaying an ionic bond.

Table XXI shows the results of this study on the alkaline earth fluorides, in which the errors quoted are twice what were observed. The short lifetime is constant within experimental error, except in the case of MgF_2 which crystallizes in a different structure. Considering those crystals of the fluorite structure, the independence of τ_1 from the cation radius is noted. This is consistent with the results on the alkali fluorides, all of which have the NaCl structure.

The anomalous lifetime shows a decreasing trend with increasing cation radius. The positron long lifetime in MgF_2 appears to be in line with this behavior. Ignoring the differences between the rutile and

fluorite crystal structures, the ratio of the alkaline earth ion radius to the fluoride ion radius and the interionic distance were used as the independent variables in the regression analysis which was previously applied to the alkali halides. The results of these quantitative analyses are shown in Tables XXIII through XXVIII, using the constants given in Table XXII.

TABLE XXI

EXPERIMENTAL RESULTS ON THE ALKALINE EARTH FLUORIDES

	Structure	$\tau_1 \times 10^{10}$ sec.	$\tau_2 \times 10^{9}$ sec.	I_2 (%)
MgF_2	rutile	2.83 ± 0.14	2.39 ± 0.08	37 ± 2
CaF_2	fluorite	3.11 ± 0.14	2.05 ± 0.08	34 ± 2
SrF_2	fluorite	3.35 ± 0.12	1.53 ± 0.08	41 ± 2
BaF_2	fluorite	3.37 ± 0.08	1.07 ± 0.08	52 ± 3

TABLE XXII

CATION-ANION RATIOS AND INTERIONIC DISTANCES OF THE ALKALINE EARTH FLUORIDES

	(r_+/r_-) (79)	Interionic Distance (45) $\times 10^8$ cm.
MgF_2	0.59	2.02
CaF_2	0.80	2.36
SrF_2	0.93**	2.50
BaF_2	1.08	2.68

**This ratio was calculated from the tables listed in Reference (79), p. 192, applying the ionic radius correction corresponding to a coordination number of 8.

The regression model for τ_1 in the alkaline earth fluorides is given by the equation

$$\tau_1 = c_o + c_1(r_{int}) + c_2(r_{int})^2 \qquad (46)$$

where $c_o = -1.47393 \times 10^{-10}$ sec.,

$c_1 = 3.07742 \times 10^{-2}$ sec/cm.,

and $c_2 = -0.47068 \times 10^{6}$ sec/cm.^{2}

TABLE XXIII

REGRESSION MODEL RESULTS FOR τ_1
ALKALINE EARTH FLUORIDES

	Actual $\times 10^{10}$ sec.	Predicted $\times 10^{10}$ sec.	Deviation
MgF_2	2.83	2.82190	0.00810
CaF_2	3.11	3.16728	-0.05728
SrF_2	3.35	3.27787	0.07213
BaF_2	3.37	3.39295	-0.02295

TABLE XXIV

STATISTICAL LEVELS FOR τ_1 REGRESSION MODEL
ALKALINE EARTH FLUORIDES

Parameter	F	Error Probability
r_{int}	32.1831	0.033
$(r_{int})^2$	0.2346	0.732

The regression model for τ_2 in the alkaline earth fluorides is given by the equation.

$$\tau_2 = c'_o + c'_1(r_+/r_-)^2 + c'_2(r_{int})^2 \qquad (47)$$

where $c'_o = 2.20149 \times 10^{-9}$ sec.,

$c'_1 = -2.69170 \times 10^{-9}$ sec.,

and $c'_2 = 0.27559 \times 10^{7}$ sec/cm^2.

TABLE XXV

REGRESSION MODEL RESULTS FOR τ_2
ALKALINE EARTH FLUORIDES

	Actual $\times 10^9$ sec.	Predicted $\times 10^9$ sec.	Deviation
MgF_2	2.39	2.38904	0.00096
CaF_2	2.05	2.01375	0.03625
SrF_2	1.53	1.59590	-0.06590
BaF_2	1.07	1.04131	0.02869

TABLE XXVI

STATISTICAL LEVELS FOR τ_2 REGRESSION MODEL
ALKALINE EARTH FLUORIDES

Parameter	F	Error Probability
$(r_+/r_-)^2$	140.2918	0.018
$(r_{int})^2$	1.1906	0.490

The regression model for I_2 in the alkaline earth fluorides is given by the equation

$$I_2 = c''_o + c''_1(r_+/r_-)^2 + c''_2(r_+/r_-)(r_{int}) \quad (48)$$

where $c''_o = 74.61369$,

$c''_1 = 214.09277$,

and $c''_2 = -94.09178 \times 10^8/cm.$

TABLE XXVII

REGRESSION MODEL RESULTS FOR I_2
ALKALINE EARTH FLUORIDES

	Actual (%)	Predicted (%)	Deviation
MgF_2	37	37.00080	-0.00080
CaF_2	34	33.98779	0.01221
SrF_2	41	41.01915	-0.01915
BaF_2	52	51.99226	0.00774

TABLE XXVIII

STATISTICAL LEVELS FOR I_2 REGRESSION MODEL
ALKALINE EARTH FLUORIDES

Parameter	F	Error Probability
$(r_+/r_-)^2$	5.2146	0.184
$(r_+/r_-)(r_{int})$	16800.7385	~0.000

The interionic distance seems to have a marked effect upon τ_1. This can be reconciled with the previous remarks, since the alkaline earth ions are small, the fluoride ion would still contribute largely to the magnitude of r_{int}. From Table XXV, it is seen that the dominant factor affecting τ_2 is the cation radius, which comes into the equation as a square function. It should be noted that the same effect was observed in the case of the alkali fluoride series. The intensity of the anomalous lifetime appears to be largely influenced by the same parameter affecting τ_2. The anomalously large F-level of the second parameter in Table XXVIII is difficult to interpret. Since this variable entered into the regression equation as the second parameter, its effect on I_2 is less than the effect of $(r_+/r_-)^2$. It should be mentioned however, that an unreasonably large partial correlation coefficient was obtained, the cause of which has escaped detection.

Presentation of Graphs. A comparison of the prompt curves used in this work, aluminum and cobalt-60, is shown in Figure 7. These runs were obtained with the same counter settings. It is seen that the widths at half-height are not too different. The aluminum prompt curve shows a tail with respect to cobalt-60 as expected, since the positron lifetime in aluminum is long compared to the lifetime of the nuclear excited states in cobalt. The peaks were made to fall on the same channel for the purpose of comparing the slopes of the time spectra.

Figures 8 and 9 both show the oxygenated and de-oxygenated time spectra in isopropylbenzene and tert-butylbenzene, respectively. In each of these diagrams, the linear "tail" corresponding to the de-oxygenated sample was adjusted so that it could be plotted on the same time calibration as the oxygenated sample. This was done merely for a

visual comparison to show the effect of oxygen on the anomalous lifetime component.

Time distribution curves in KF, KCl, LiF, and CsF are shown in Figures 10-13. Figure 14 shows the annihilation spectrum in MgF_2. In each of these graphs, the corresponding prompt cobalt-60 curve was included for comparison. In some cases, the prompt curve was vertically displaced for clarity.

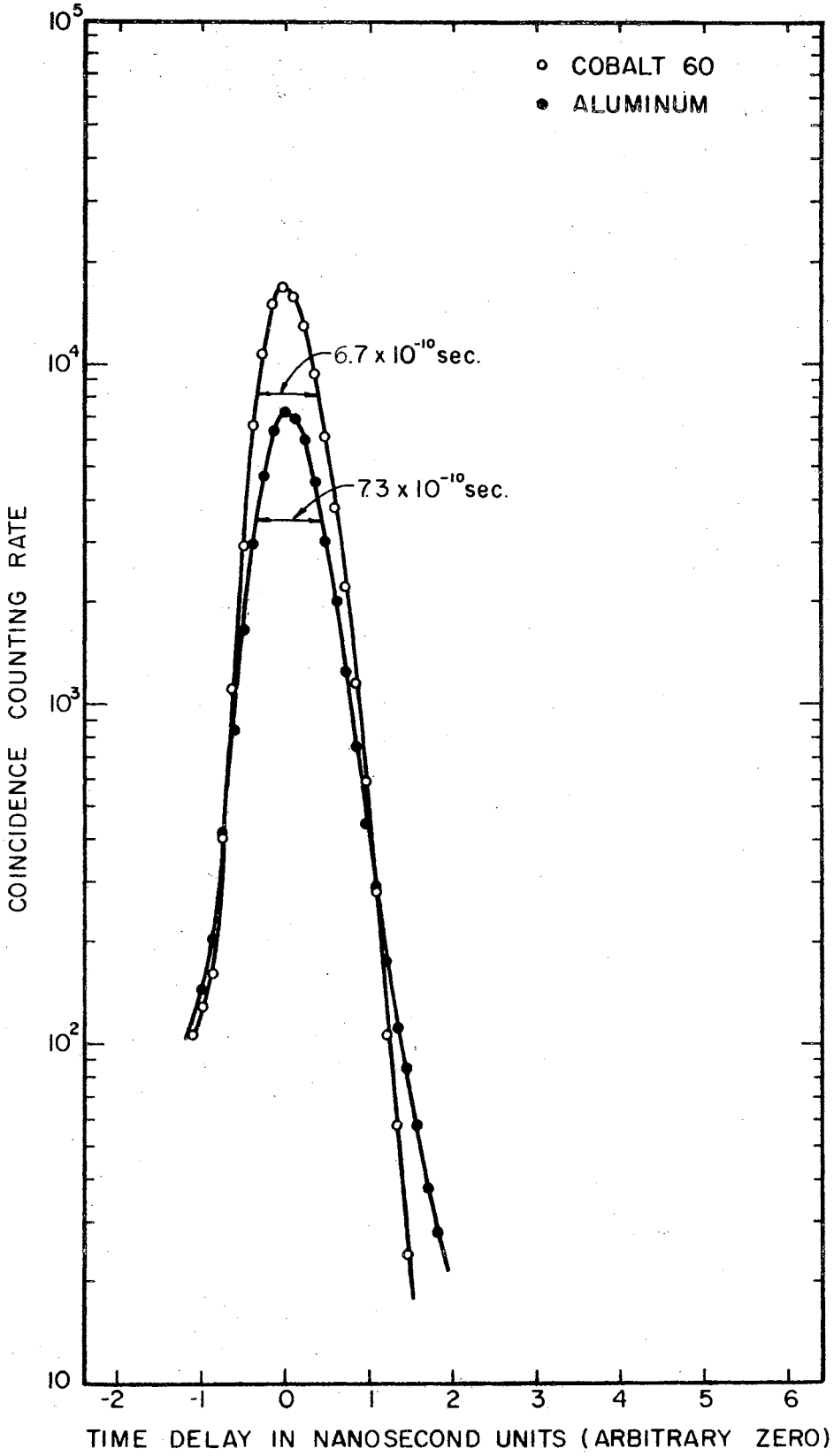

Figure 7. Comparison of the Prompt Curves

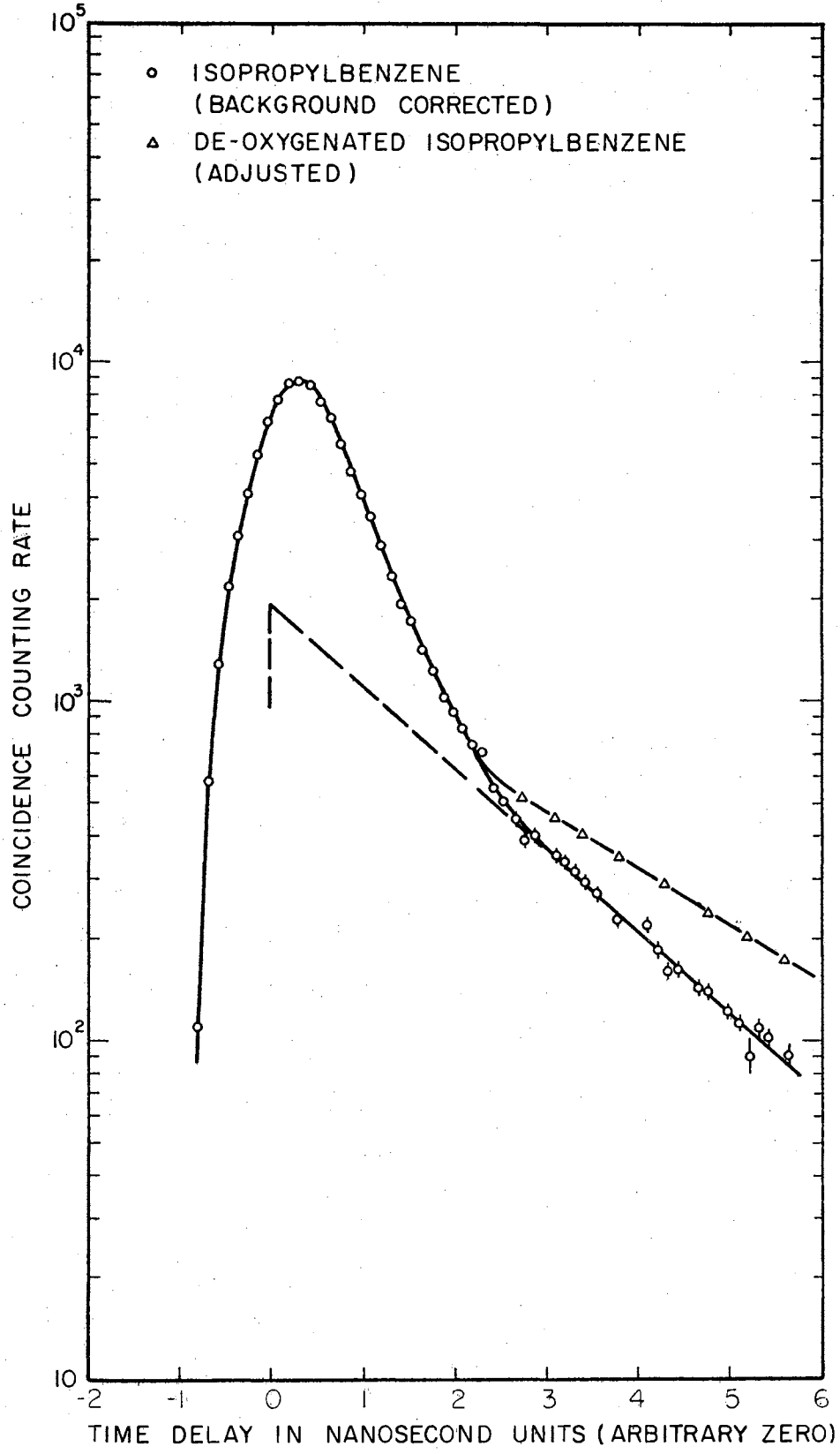

Figure 8. Annihilation Spectra in Isopropylbenzene

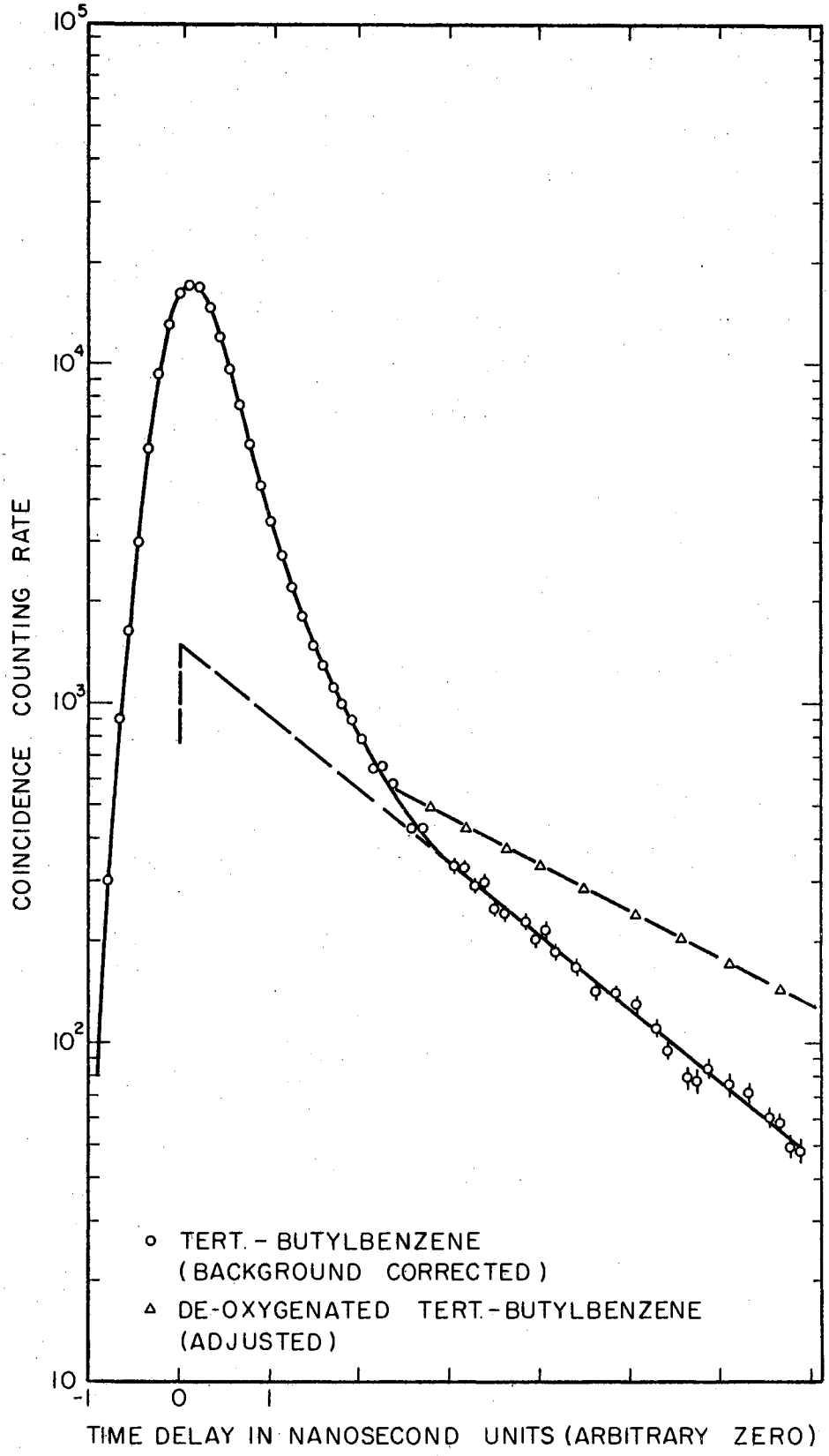

Figure 9. Annihilation Spectra in tert-Butylbenzene

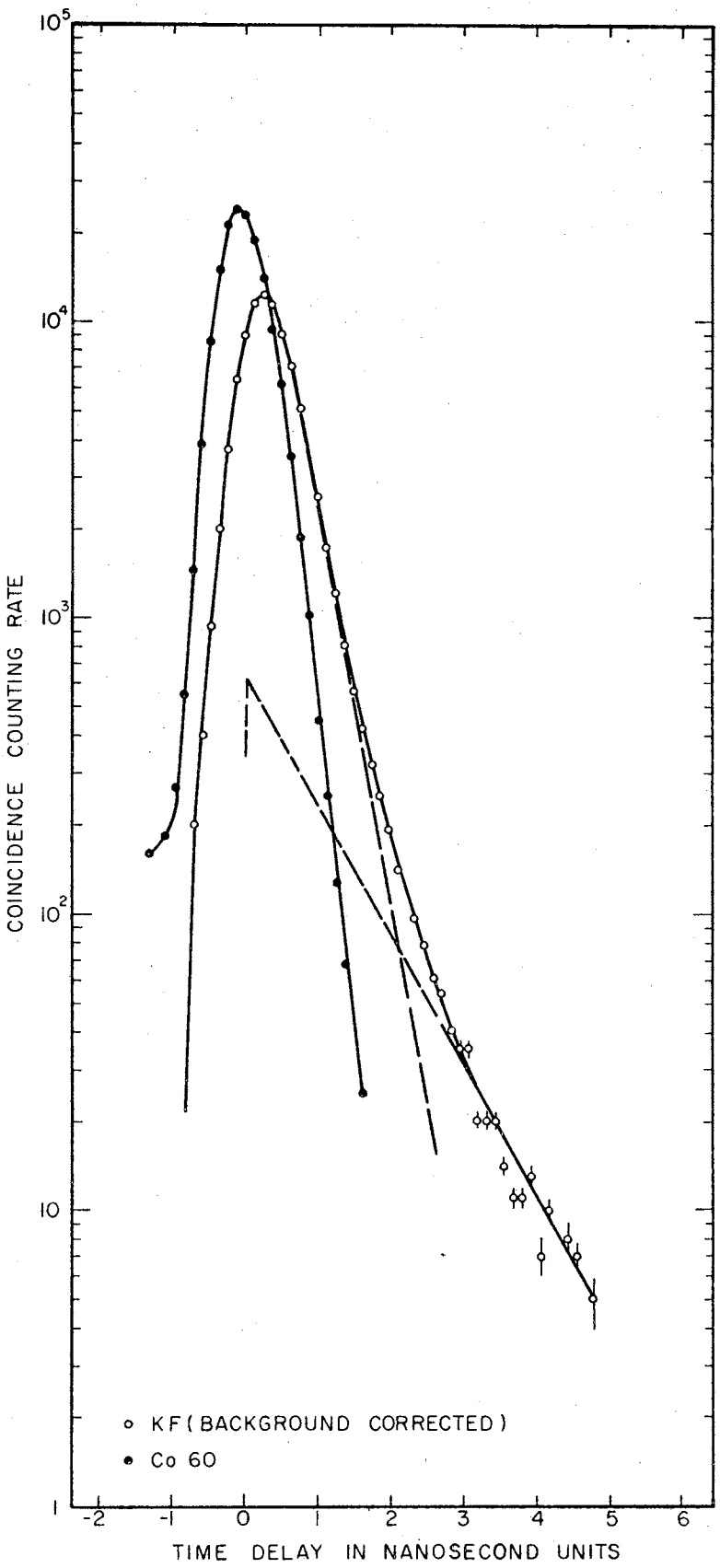

Figure 10. Annihilation Spectrum in KF

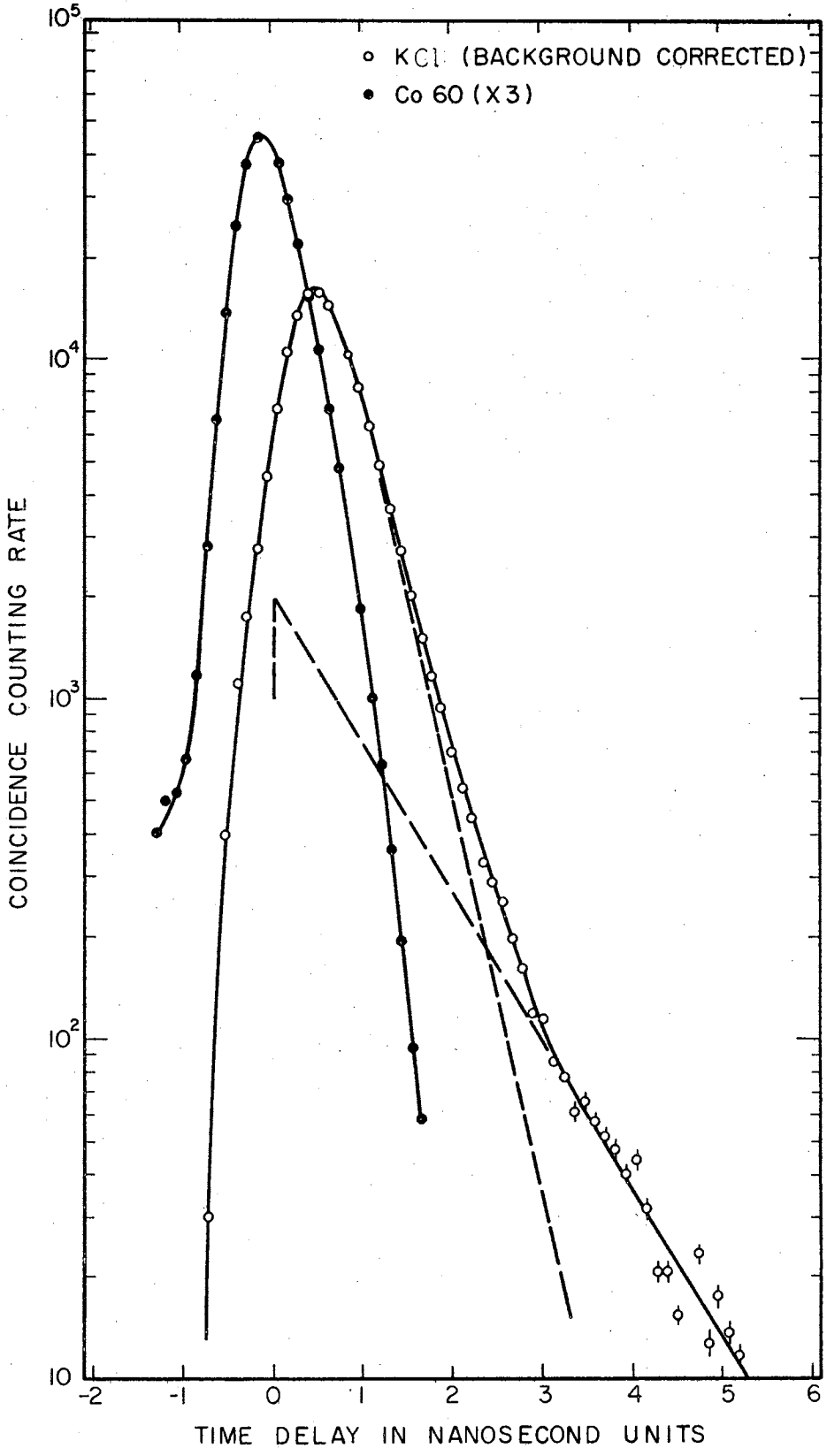

Figure 11. Annihilation Spectrum in KCl

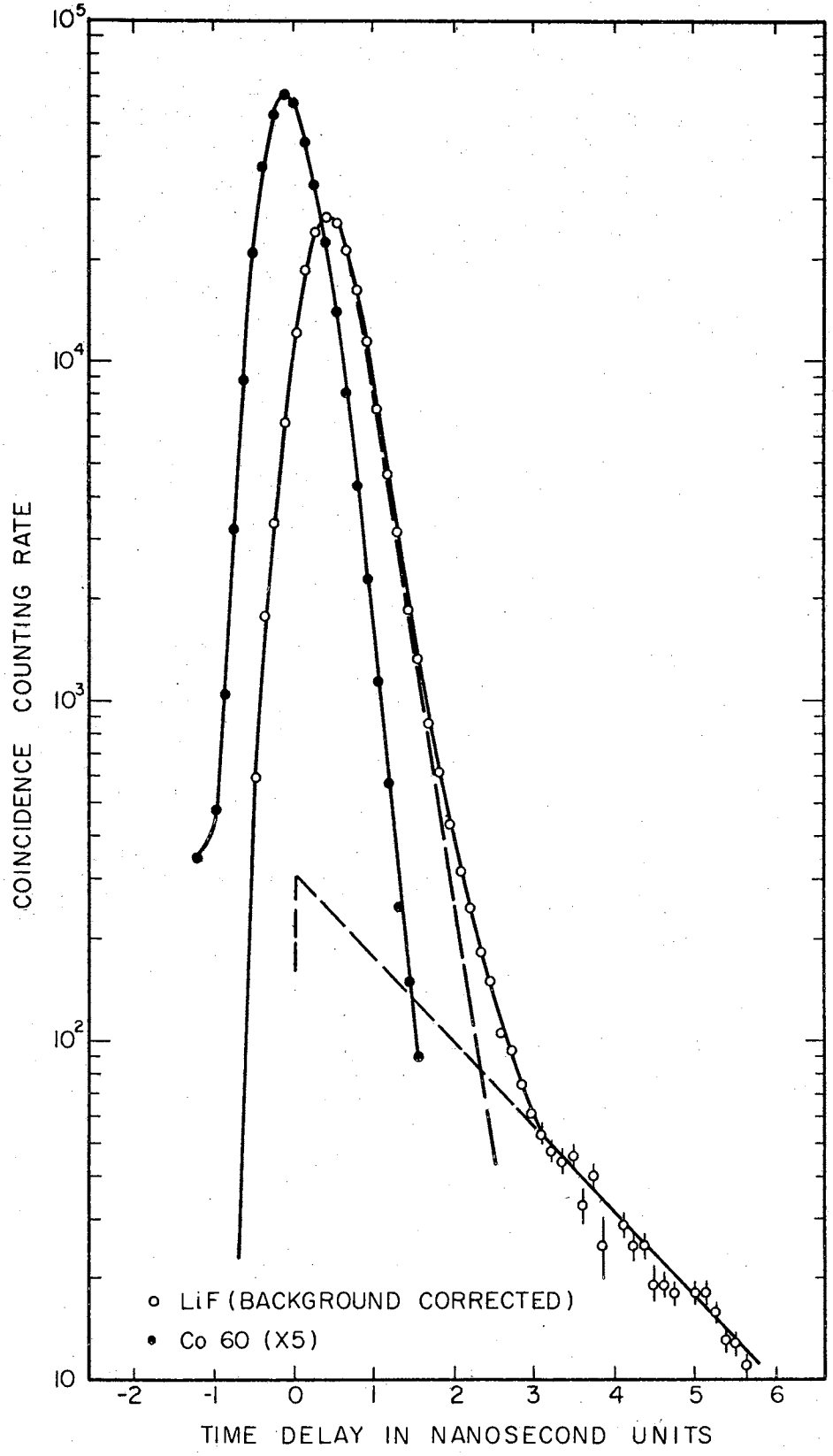

Figure 12. Annihilation Spectrum in LiF

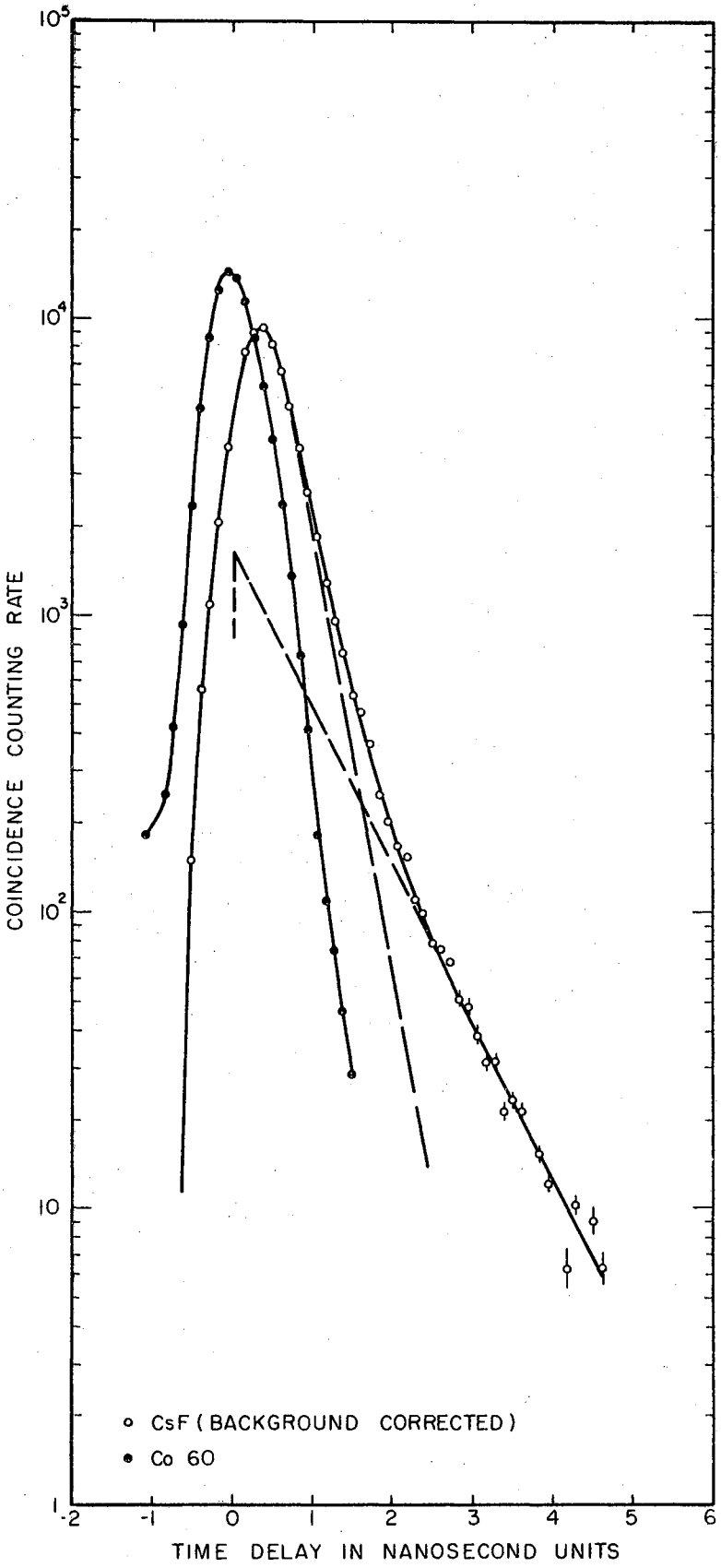

Figure 13. Annihilation Spectrum in CsF

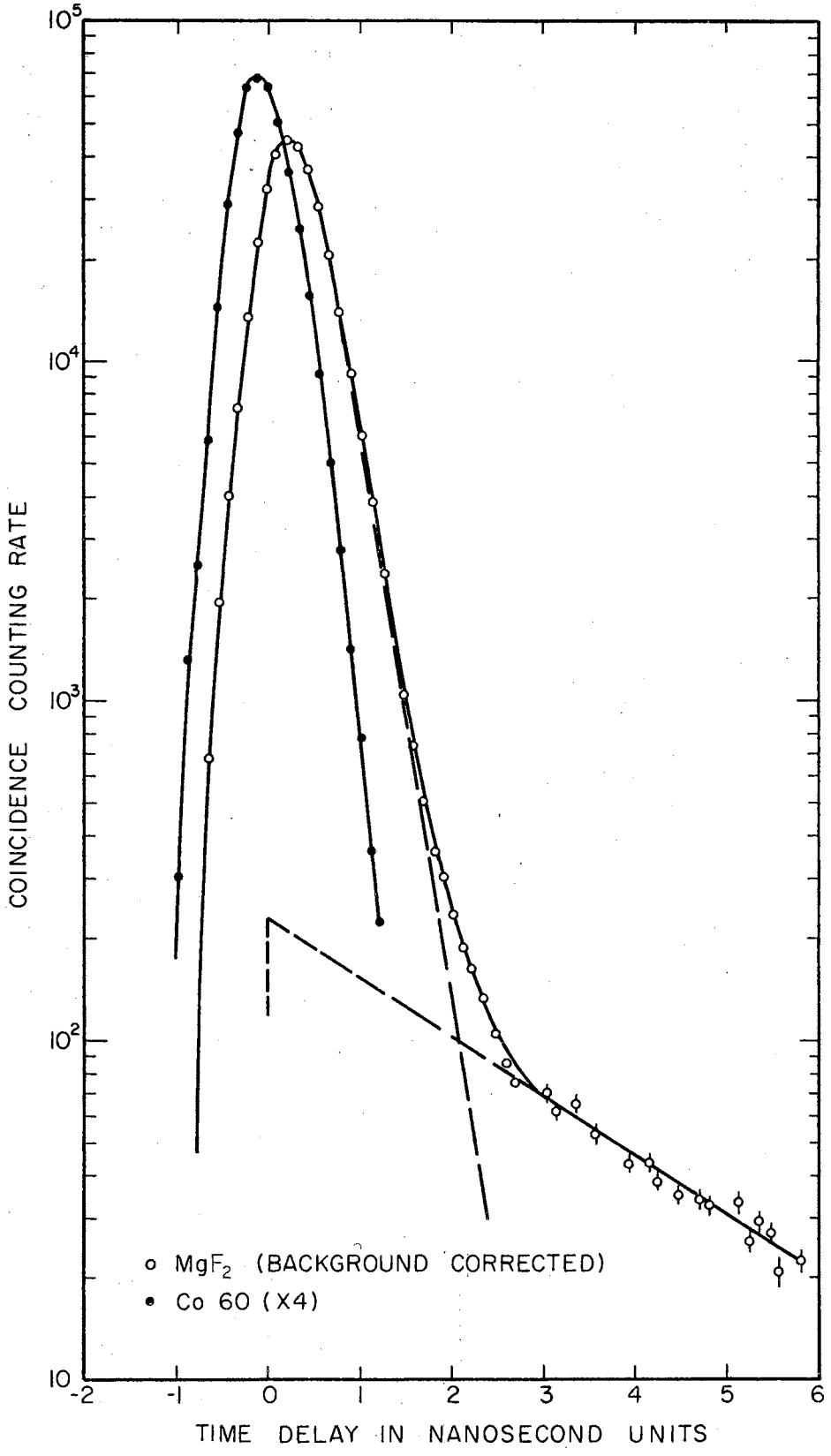

Figure 14. Annihilation Spectrum in MgF_2

Theoretical Considerations

Speculations on the Polarization of the Crystal Field due to Ps. In the absence of more definite information on the potential inside the ionic crystal, Neamtan et al. (46) assumed a more or less simple model for the potential in a LiH crystal. Presumably, their model describes in a certain average way, the potential in the crystal due to charges of ions, as well as dipole and higher moments. We present below a qualitative argument that effects on lifetime due to polarization of the crystal field may not be attributed to the neutral positronium atom, arising from dipole-dipole interactions, but rather, to the positron, in agreement with their explanations.

If the polarizability of the material and therefore, its dielectric constant, is to affect the lifetime of positronium in it, this would be due to a change in the polarization (dipole moment per unit volume) induced by the presence of Ps. That is, the induced polarization changes the field at the site of the positronium atom and the field affects the energy levels and wavefunction, hence, the lifetime of the quasi-bound state. Since we are dealing with electromagnetic interactions, this would be of the order of α^2 or e^4, where α is the fine structure constant and e refers to the electron charge. The first α would be for the Ps atom to change dipole moment density, another α would be needed for the changed dipole moment density to affect positronium.

The S state ($l = 0$) of a hydrogen-like atom has no dipole moment. Since the Ps atom is neutral, only those higher states which have dipole moments can cause a change in polarization. If, indeed, one has

a higher state which has non-vanishing dipole moment and if this changes the polarization of the crystal which ultimately changes the field at the position of the positronium atom, this would cause a change in the lifetime of this higher state. However, before annihilation can occur, the Ps atom would radiate optically to the ground state (13). Each transition to a lower level involves at least an order α in the dipole transition approximation. One would therefore have an effect of at least α^3. This effect is at least two orders of α smaller than the fine and hyperfine effects, which are of equal magnitude in the case of Ps.

From the above argument, we would be dealing with an effect $\alpha^2 \sim (1/137)^2 \sim 10^{-4}$ orders of magnitude less than the spin-orbit and spin-spin interactions. Inasmuch, the polarization of the crystal field due to positronium may therefore be neglected. However, it is possible that changes in the crystal polarization may be attributed to the positrons upon entering the medium and in the course of their slowing down to thermal velocities. In this case, the positrons are said to be in polaron states; i.e., states in which positrons are surrounded by a phonon cloud due to lattice polarization. This is analogous to the theoretical treatment of positrons annihilating in metals, in which the electron plasma may not be neglected.

Calculations of Positron Lifetimes in Alkali Fluorides. The theoretical aspect of the problem of positrons annihilating in an ionic medium is complicated by the lattice polarization caused by the positron's electric field. The distortion of the electronic configuration may be approximated by the inclusion of the dielectric constant of the crystal for static fields in the wavefunction or wavefunctions for any feasible treatment. The following analysis was applied to interstitial ions (49).

Considering the positron plus anion, Gol'danskii et al. (49) calculated the positron lifetimes in some alkali fluorides using the analytical wavefunction for the fluoride ion obtained by Brown (80), where the energy is minimized with respect to the radial function, subject to the condition of orthonormality. Similar theoretical calculations were carried out in this work to predict positron lifetimes in LiF, NaF and KF using known dielectric constants. This approximation takes into consideration the formation of a bound system (e^+F^-) in which the fluoride ion acts as the nucleus, so that one must have a bound state wavefunction to describe the positron polaron.

The positron wavefunction, χ, used is that obtained by Gol'danskii et al. (49), using the variational method. For the fluoride ion, the wavefunction, Ψ, is given by the equations below:

$$1s: \quad f_1 = 51.77\, re^{-8.75r}$$

$$2s: \quad f_2 = 11.55 \left[re^{-7.25r} - r^2(1.03e^{-3.33r} + 0.300e^{-1.9r}) \right]$$

$$2p: \quad f_3 = 13.57\, r^2(e^{-3.86r} + 0.133e^{-1.36r})$$

where

$$f(n,r) = rR(n,l)$$

and $$\Psi = R(n,l)\, Y(\theta, \varphi). \tag{49}$$

The positron wavefunction for the 1s polaron state is given by

$$\chi = Ae^{-\alpha r} \tag{50}$$

where

$$\alpha = \frac{1}{16}\left(\frac{5}{\epsilon_o} + \frac{11}{\epsilon}\right) \quad \text{and} \quad A = \frac{\alpha^3}{\pi}\,.$$

The constant ϵ_o refers to the dielectric constant of the material when the ions are fixed in their normal equilibrium position and ϵ refers to the dielectric constant for the static field of the positron and anion.

Using Equation (33),

$$\bar{\rho} = \sum_i \left| \int \Psi_i^*(\vec{r}) \Psi_i(\vec{r}) \, \chi^* \chi \, d\tau \right| .$$

Substituting for Ψ and χ ,

$$\bar{\rho} = \sum_i \left| \int R^2(n,1) \, Y^*(\theta,\varphi) Y(\theta,\varphi) e^{-2\alpha r} \, r^2 \, \sin\theta \, d\theta \, d\varphi \, dr \right| .$$

Using the orthonormality condition for spherical harmonics given by

$$\int Y^*(\theta,\varphi) Y(\theta,\varphi) \, d\Omega = K = \text{constant}, \tag{51}$$

$\bar{\rho}$ reduces to

$$\bar{\rho} = K \sum_i \left| \int_o^\infty f^2(n,r) \, e^{-2\alpha r} \, dr \right| ,$$

where integration to infinity takes into account the effect on the entire crystal. It is easily seen that the largest contribution to $\bar{\rho}$ comes from f_1. From Equation (34), τ is inversely proportional to the electron density at the position of the positron. The smallest contribution to τ then comes from f_1. This is actually what one would expect since the 1s electrons are more tightly bound to the nucleus, being in a region of high electrostatic potential.

From Equation (34),

$$\tau = 5 \times 10^{-10} \frac{\bar{\rho}_o}{\bar{\rho}} ,$$

where $\bar{\rho}_o = 1/8\pi a_o^3$, the electron density in the positronium atom averaged over the initial spin states; a_o refers to the Bohr radius. The

method outlined above was applied to LiF, NaF, and KF; CsF was omitted due to the unavailability of constants describing its dielectric properties. The values used for ϵ_o come from the square of the index of refraction of the crystal and ϵ are those due to static fields or for radio frequencies. These constants are shown in Table XXIX, together with the ratios based on the respective τ_{LiF} of both experimental and theoretical results obtained in this work.

TABLE XXIX

POSITRON LIFETIME RATIOS IN e^+-F^- BOUND SYSTEMS

	ϵ_o (81)	ϵ (81)	Experimental τ_1/τ_{LiF}	Experimental τ_2/τ_{LiF}	Theoretical (τ/τ_{LiF}) Gol'danskii et al. (49)	Theoretical (τ/τ_{LiF}) This Work
LiF	1.92	9.27	1.00	1.00	1.00	1.00
NaF	1.74	6.00	0.91	1.16	0.61	0.56
KF	1.85	6.05	1.00	0.66		0.63

From the results of Gol'danskii et al. (49) shown in Table V, positron lifetimes are seen to vary with the halogen ion. From the analyses of the results of the anomalous lifetimes in this work, these theoretical results should be used to predict τ_2, although the 1s positron polaron wavefunction was used. Comparing the theoretical values with τ_2, agreement is obtained in the case of KF, whereas the experimental result on NaF is greater by about a factor of 2.

The selection of either the positron or the fluoride wavefunction may be wrong in these calculations. The use of the 1s polaron wavefunction suggests that the above calculations predict τ_1, in which case

no agreement is attained. However, the F^- wavefunction may not describe exactly the wavefunction of an interstitial ion, since one would expect the energy levels of an interstitial ion to be different from the bands of the crystal. Since it is known that Schottky defects dominate over Frenkel defects in alkali halide crystals, it is plausible that positron capture is due to halogen ions in normal lattice positions rather than in interstitial positions, unless the crystals are injected with impurities. It is seen, however, that the polarization of the lattice may be approximated by the inclusion of the dielectric constants in the polaron wavefunction.

Summary of Results and Conclusions

The findings of this study on some alkylbenzenes show that positron annihilation experiments can be used as a method in determining the electron donating abilities of substituents to the benzene ring. However, due care must be observed especially in compounds which possess high oxygen solubilities. De-oxygenation is recommended for such liquids, since the unpaired electrons in the paramagnetic oxygen molecule are capable of perturbing the annihilation processes. The rapid quenching of ortho-Ps states due to the presence of oxygen may be attributed to the formation of the complex $(e^+e^-)O_2$ and subsequent annihilation by the pickoff process. At very low oxygen concentrations, the formation of water molecules inhibits positrons in the triplet bound state from annihilating by the pickoff mechanism.

It has been observed that dissolved oxygen has a very slight effect on the amount of orthopositronium formed. A small effect of chain length of the alkyl substituent on τ_2 was also noted, although the

behavior cannot be reconciled with the findings of Gray et al. (82), in which τ_2 was found to decrease with increasing hydrocarbon chain length.

This work confirms that positrons annihilating in ionic crystals are capable of forming Ps atoms, as evidenced by the complex annihilation time spectrum. It has been observed that the halide ion is the predominant factor responsible for the short lifetime, whereas the alkali ion has a greater influence on the anomalous lifetime. The results of the calculations show a square dependence of τ_1 on anion radius rather than a cubic relation as predicted by Ferrell (20). The anomalous lifetime and its intensity are both affected by the cation radius as seen from the quadratic relations given by the linear regression models. The results on τ_2 are in disagreement with the empirical relation obtained by Bisi et al. (48) given in Equation (31), which shows a square dependence on anion radius.

It has been observed that positron decay in alkaline earth fluorides involves the formation of positron-bound systems, and that the alkaline earth ionic crystals were seen to exhibit longer anomalous lifetimes than the alkali halides considered. This may be attributed to the fact that the electron densities in the former are smeared over a larger volume, due to the divalent character of the cations.

The lifetimes of positrons annihilating from the positron-anion (e^+F^-) bound state, using the 1s positron polaron wavefunction and assuming a wavefunction for the fluoride ion, were calculated. In the approximations where the static dielectric constant ϵ describes the lattice polarization due to the presence of the positron and taking the lifetime ratios in terms of lithium fluoride, the results were found to be in agreement with the anomalous lifetime measurement in the case

of KF.

Suggestions for Further Work

It would be interesting to carry out further positron lifetime measurements in de-oxygenated organic compounds in order to determine quantitatively the effects of polar substituents to the benzene ring. It is plausible that with more available data, force constants of various chemical bonds may be measured through the properties of the annihilation processes. It is likely that this experimental method can be used in the future as a means of identifying organic compounds, or determining oxygen concentrations and solubilities in such liquids, assuming second order kinetics to hold, so that a relation such as Equation (30) may be suitable.

More experimental data are needed to eliminate the disagreement among existing measurements of positron lifetimes and intensities in alkali halides. Also, it would be informative to observe the effect on positron lifetimes, of increasing concentrations of crystal defects caused by vacancies, impurity ions, F-centers, and neutron irradiation, so that a meaningful comparison with theoretical predictions may be carried out.

BIBLIOGRAPHY

1. Berko, S. and F. Hereford: Reviews of Modern Physics, 28: 299 (1956).

2. Dirac, P. A. M.: Proceedings Cambridge Philosophical Society, 26: 361 (1930).

3. Heitler, W.: The Quantum Theory of Radiation, (Oxford University Press, New York and London, 1936) p. 114.

4. Jauch, J. M. and F. Rohrlich: The Theory of Photons and Electrons, (Addison-Wesley, Reading, Massachussetts, 1955) p. 263.

5. Thibaud, J.: Physical Review, 45: 781 (1934).

6. Joliot, F.: Comptes Rendues, 197: 1622 (1933).

7. Klemperer, O.: Proceedings Cambridge Philosophical Society, 30: 374 (1934).

8. Alichanian, A. I., A. I. Alichanov and L. A. Arzimowich: Nature, 137: 703 (1936).

9. Beringer, R. and C. G. Montgomery: Physical Review, 61: 222 (1942).

10. Yang, C. N.: Physical Review, 77: 242 (1950).

11. DeBenedetti, S. and H. C. Corben: Annual Review of Nuclear Science, 4: 191 (1954).

12. Wallace, P. R.: Solid State Physics, 10: 1 (1960).

13. Ore, A. and J. L. Powell: Physical Review, 75: 1696 (1949).

14. Deutsch, M.: Physical Review, 82: 455 (1951).

15. Bell, R. E. and R. L. Graham: Physical Review, 90: 644 (1953).

16. DeBenedetti, S., C. E. Cowan, W. R. Konneker and H. Primakoff: Physical Review, 77: 205 (1950).

17. Garwin, R. L.: Physical Review, 91: 1571 (1953).

18. Lee-Whiting, G. E.: Physical Review, 97: 1557 (1955).

19. Mandansky, L. and F. Rasetti: Physical Review, 79: 397 (1950).

20. Ferrell, R. A.: Reviews of Modern Physics, 28: 308 (1956).

21. Pond, T. A.: Physical Review, 93: 478 (1954).

22. Simons, L.: Physical Review, 90: 165 (1953).

23. Gittelman, B., E. P. Dulit and M. Deutsch: Bulletin of the American Physical Society, 1: 69 (1956).

24. Wheeler, J. A.: Annals of the New York Academy of Science, 48: 221 (1946).

25. Green, R. E. and R. E. Bell: Canadian Journal of Physics, 35: 398 (1957).

26. Ore, A.: Univ. Bergen Arbok, No. 9 (1949).

27. Brandt, W., S. Berko and W. Walker: Physical Review, 120: 1289 (1960).

28. Gerholm, T. R.: Arkiv für Physik, 10: 523 (1956).

29. Deutsch, M. and S. Berko: Positron Annihilation and Positronium: Seigbahn K., ed.,: Alpha-Beta- and Gamma Ray Spectroscopy. Vol. II, (Interscience Publishers, New York, 1965) p. 1583.

30. Green, J. and J. Lee: Positronium Chemistry, (Academic Press, New York, 1964) Chapters V and VII.

31. Paul, D. A. L.: Canadian Journal of Physics, 37: 1059 (1959).

32. Lee, J. and G. J. Celitans: Journal of Chemical Physics, 42: 437 (1965).

33. Kerr, D. P., A. M. Cooper and B. G. Hogg: Canadian Journal of Physics, 43: 963 (1965).

34. Bell, R. E. and R. L. Graham: Physical Review, 90: 644 (1953).

35. Bell, R. E. and M. H. Jørgensen: Canadian Journal of Physics, 38: 652 (1960).

36. Kahana, S.: Physical Review, 117: 123 (1960).

37. Kahana, S.: Physical Review, 129: 1622 (1963).

38. Kanazawa, H., Y. H. Ohtsuki and S. Yanagawa: Progress of Theoretical Physics, 33: 1010 (1965).

39. Carbotte, J. P.: Physical Review, 144: 309 (1966).

40. Held, A. and S. Kahana: Canadian Journal of Physics, 42: 1908 (1964).

41. Kanazawa, H., Y. H. Ohtsuki and S. Yanagawa: Physical Review, 138: 1115 (1965).

42. Kehonen, T.: Annalen de Academie Scienciae Fennicase, 6: 130 (1963).

43. Weisberg H. and S. Berko: Physical Review, 154:249 (1967).

44. Kittel, C.: Introduction to Solid State Physics, (John Wiley & Sons, New York, 1961) Chapter I.

45. Pauling, L.: The Nature of the Chemical Bond, (Cornell University Press, New York, 1960) Chapter XIII.

46. Neamtan, S. M. and R. I. Verall: Physical Review, 134: 1254 (1964).

47. Bisi, A., A. Fiorentini and L. Zappa: Physical Review, 131: 1023 (1963).

48. Bisi, A., A. Fiorentini and L. Zappa: Physical Review, 134: 328 (1964).

49. Gol'danskii, V. I. and E. P. Prokop'ev: Soviet Physics-Solid State, 6: 2641 (1965).

50. Lang, L. G. and S. DeBenedetti: Physical Review, 108: 914 (1957).

51. Millett, W. E. and R. Castillo-Bahena: Physical Review, 108: 257 (1957).

52. Stewart, A. T. and N. K. Pope: Physical Review, 120: 2033 (1960).

53. Verheijke, M. L.: Nuclear Instruments and Methods, 34: 132 (1965).

54. Gilroy, D. and J. E. O. Mayne: Journal of Applied Chemistry, 12: 382 (1962).

55. Arthur, P.: Analytical Chemistry, 36: 701 (1964).

56. Oeschlager K.: Unpublished M. S. Thesis, Oklahoma State University, 1965.

57. Melton, B. F. and V. L. Pollak: Bulletin of the American Physical Society, Serial II, 11: 32 (1966).

58. Blichiarski, J., J. W. Hennel, K. Kynicki, J. Mikulski, T. Waluga and G. Zapolski: Arch. d. Scien., 11: 243 (1958).

59. Bell, R. E. and H. E. Petch: Physical Review, 76: 1409 (1949).

60. Bell, R. E.: Coincidence Techniques and the Measurement of Short Mean Lives: Siegbahn, K. ed.,: Alpha-Beta- and Gamma Ray Spectroscopy. Vol. II, (Interscience Publishers, New York, 1965) p. 905.

61. Kerr, D. D. and B. G. Hogg: The Review of Scientific Instruments, 33: 391 (1962).

62. Simms, P. C.: The Review of Scientific Instruments, 32: 894 (1961).

63. Schwarzchild, A.: (Invited paper at the Conference of Electromagnetic Lifetimes and Properties of Nuclei, Gatlinburg, Tennessee, U. S. A., Oct. 5-7, 1961), issued as Brookhaven report, BNL: 5715 (Sept. 25, 1961).

64. Ledezma, A. Z.: Unpublished M. S. Thesis, Oklahoma State University (1966).

65. Hatcher, C. H., W. E. Millett and L. Brown: Physical Review, 111: 12 (1958).

66. Bay, Z.: Physical Review Letters, 77: 419 (1950).

67. Bacon, R. H.: American Journal of Physics, 21: 428 (1953).

68. Zimmerman, W.: The Review of Scientific Instruments, 32: 1063 (1961).

69. Ostle, B. Statistics in Research: (The Iowa State University Press, Iowa, 1964) pp. 177-190, 529-543.

70. Newman, M. S.: Steric Effects in Organic Chemistry, (John Wiley and Sons, New York, 1956) p. 169.

71. Pagilagan, R.: Private Communication.

72. Gourary, B. S. and F. J. Adrian: Solid State Physics, (Academic Press, Inc., New York, 1960). Vol. 10, p. 143.

73. Pollak, B. L.: Unpublished Ph.D. Dissertation, Washington University (1961).

74. Dekker, A. J.: Solid State Physics, (Prentice Hall, Inc., New Jersey, 1963) p. 126.

75. See Reference 74, p. 122.

76. Bisi, A., C. Bussolatti, S. Cova and L. Zappa: Physical Review, 141: 348 (1966).

77. Mellor, J. W.: Comprehensive Treatise on Inorganic and Theoretical Chemistry, (John Wiley and Sons, Inc., New York, 1961) Vol. 2, Supplement 2, p. 174.

78. Bussolatti, C. and L. Zappa: Physical Review, 136: 657 (1964).

79. Zhdanov, G. S.: Crystal Physics, (Academic Press, New York, 1965) p. 196.

80. Brown, F. W.: Physical Review, 44: 214 (1933).

81. Mott, N. F. and R. W. Gurney: Electronic Properties in Ionic Crystals, (Oxford at the Clarendon Press, Great Britain, 1948) p. 12.

82. Gray, P. R., G. P. Sturm and C. F. Cook: Journal of Chemical Physics, 46: 3487 (1967).

APPENDIX A

GAUSSIAN FIT - CENTROID CALCULATION

$y(x_i)$ = no. of counts in ith channel

n = no. of points on semi-Gaussian curve

$m = n - 2$

$$y(x_i) = y_o\, e^{-(x_i - x_o)^2/2\sigma^2}$$

$$y(x_i - 1) = y_o\, e^{-\left[(x_i - 1) - x_o\right]^2/2\sigma^2}$$

$$y(x_i + 1) = y_o\, e^{-\left[(x_i + 1) - x_o\right]^2/2\sigma^2}$$

$$Q_i = \frac{y\,(x_i - 1)}{y\,(x_i + 1)} = e^{2(x - x_o)/\sigma^2}$$

$$S_i = \ln Q_i$$

$$\text{Num} = \sum x_i \ln Q_i - \frac{\sum x_i \sum \ln Q_i}{m}$$

$$\text{Denom} = \sum x_i^2 - \frac{(\sum x_i)^2}{m}$$

$$\text{slope} = \frac{\text{Num}}{\text{Denom}} \quad ; \quad \bar{S} = \frac{\sum S_i}{m} \quad \text{and} \quad \bar{x} = \frac{\sum x_i}{m}$$

$$b = \bar{S} - (\text{slope})\,(\bar{x})$$

centroid = x-intercept = b/slope

VITA

Concepcion V. San Jose

Candidate for the Degree of

Doctor of Philosophy

Thesis: POSITRON LIFETIME MEASUREMENTS IN SOME IONIC CRYSTALS AND SOME ALKYLBENZENES

Major Field: Physics

Biographical:

Personal Data: Born August 3, 1940, in Manila, Philippines, the daughter of Sarah V. and Manuel V. San Jose.

Education: Attended grade school in Manila, Philippines; graduated from St. Scholastica's College, Manila, Philippines, in 1955; received the Bachelor of Science degree with a major in Physics from the University of the Philippines, Diliman, Rizal, Philippines, in 1959; received the Master of Science degree with a major in Physics from Purdue University, W. Lafayette, Indiana, in 1963; completed the requirements for the Doctor of Philosophy degree in July, 1967.

Professional experience: Was assistant instructor in physics at the University of the Philippines, 1959-1960; graduate teaching assistant in mathematics at Purdue University, 1962; graduate teaching assistant in physics at Oklahoma State University, 1963-1967; graduate research assistant at Oklahoma State University, summers 1965-1967.

Organizations: Sigma Pi Sigma and American Association of University Professors.

Date of Final Examination: July, 1967